

Giorgos Leloudas  
s041550

# Optimization of Wind Turbines with respect to Noise



Master's Thesis Project supervised by  
Jens N. Sørensen  
Søren Hjort  
Wen Zhong Shen  
Wei Jun Zhu

*November 2006*

MEK, **DTU**  
in collaboration with SIEMENS WIND POWER A/S

## **Acknowledgments**

I would like to thank all my supervisors, Jens N. Sørensen, Wen Zhong Shen and Wei Jun Zhu at DTU and Søren Hjort at SIEMENS WIND POWER A/S for valuable discussions and advice. Also SIEMENS WIND POWER A/S for making this project possible and Ejler Kristensen for his participation and guidance throughout the measurement campaign and for pre-processing the data files to 10 sec averages.

## **Abstract**

The purpose of this thesis is to examine the issue of noise from wind turbines and eventually optimize their operation settings. The tools used are both simulations and measurements.

The programming part was based on an existing model by Wei Jun Zhu developed in DTU as part of another master thesis. The code was expanded, combined with a BEM code and coupled to an optimization routine. All simulations and tests were made on a SIEMENS SWT-2.3-92 wind turbine equipped with a B45 blade.

Noise measurements were taken at the Risø test site for large wind turbines at Høvsøre. A total of eleven hours of data were obtained in two days and they featured measuring noise versus different pitch angles and rotational velocities.

The first aim of this project was to validate the code predictions against the measurements, in a way that it had not been possible to do before. In addition, to make a detailed study of the individual noise mechanisms along the blade and with changing wind speed.

Subsequently, the code was going to be used for optimizing the performance of the SWT-2.3-92 wind turbine with respect to noise. This is a variable speed, pitch regulated machine, so the project concentrated on looking for the combinations of these settings that would lead to a possible reduction in noise by keeping the power production at high levels. Alternatively, to find the settings that optimize power production by constraining the maximum allowed noise.

The ultimate ambition was to see whether the design of the blade itself could be modified for it to become more silent. This study concentrated on the chord, twist and relative thickness distributions.

# Contents

<b>1</b>	<b>Introduction</b>	<b>1</b>
<b>2</b>	<b>The Noise Prediction Model</b>	<b>4</b>
2.1	Summary of past work . . . . .	4
2.1.1	The Boundary Layer Thickness Database . . . . .	6
2.2	The code BEM-NOISE . . . . .	7
<b>3</b>	<b>Noise Measurements Campaign Description</b>	<b>10</b>
3.1	Area Description . . . . .	10
3.2	Wind Turbine Description . . . . .	12
3.3	Meteorological Conditions . . . . .	12
3.4	Instrumentation . . . . .	12
3.5	Measurement Location . . . . .	13
3.6	Procedure . . . . .	13
3.7	Data Processing . . . . .	14
<b>4</b>	<b>Results</b>	<b>18</b>
4.1	Extensive Validation . . . . .	21
4.1.1	Against Default Operational Settings . . . . .	21
4.1.2	Against Rotational Velocity . . . . .	22
4.1.3	Against Pitch Angle . . . . .	24
4.1.4	Against Both . . . . .	27
4.1.5	Against Spectra . . . . .	27
4.1.6	Summary . . . . .	29
4.2	Rotorplane Measurements . . . . .	32
4.3	Going into some details . . . . .	35
4.3.1	Localizing the noise . . . . .	35
4.3.2	Identifying the noise . . . . .	37
<b>5</b>	<b>Optimization</b>	<b>41</b>
5.1	Wind Turbine Settings Optimization . . . . .	41

---

5.1.1	Noise Minimization . . . . .	42
5.1.2	Power Maximization . . . . .	43
5.1.3	Limitations . . . . .	44
5.2	Wind Turbine Blade Optimization . . . . .	47
5.2.1	Twist optimization . . . . .	48
5.2.2	Chord optimization . . . . .	50
5.2.3	Relative thickness optimization . . . . .	52
5.2.4	All variables optimization . . . . .	52
5.2.5	Summary . . . . .	56
<b>6</b>	<b>Conclusions</b>	<b>57</b>
<b>A</b>	<b>Optimized Settings</b>	<b>59</b>

# Chapter 1

## Introduction

One of the big challenges in the beginning of the new century is to become independent of fossil fuels. Both the increasing prices in oil and gas, but also the need to stop global warming, have forced modern states turn to renewable energies. Presently, the most cost effective and popular among these energy sources, seems to be wind energy. It is therefore not a surprise that the wind energy industry has become a flourishing sector and that it is expected to grow even more in the years to come. Wind turbines are becoming larger in size and a big concentration of them is now built off-shore. This does not mean however that the development inland will stop, while areas that are already filled to capacity are expected to repower to larger and more efficient machines.

Wind turbines provide clean, non-polluting, inexhaustible energy. In most places they are viewed with sympathy. However, one of the main concerns for future neighbors to planned winds is noise. This is not a surprise: research has shown that people are worried about noise, more than anything else, when it comes to the creation of *anything* new (ranging from roads and shopping centers to night clubs) in their vicinity.

*Noise is every unwanted sound.* So in that sense, yes, wind turbines produce unwanted sound and hence they are noisy. This is unavoidable: virtually everything with rotating parts will produce some sound. As a matter of fact, wind turbines produce noise with *two* different distinct ways: the one is *mechanical noise* from the rotating machinery in the nacelle, and the other is *aerodynamic* noise produced by the rotating blades through the air.

Wind turbines are relatively less noisy when compared to other sources of environmental noise, such as roads, airports and construction machinery. To their disadvantage, however, they are usually placed in a rural environment, where the background noise is relatively low and they can therefore be heard, while this would not be the case if they were next to a busy road. And even

in this quiet environment, at high wind speeds, the wind turbine noise gets masked from the ambient noise (trees, branches, bushes, leaves, waves, etc).

If noise was a considerable problem 20 years ago, this is no longer the case. Indeed, smaller wind turbines tended to be noisier but they have been replaced with more carefully designed MW machines. Downwind machines were also considerably noisier, but they are outdated today for a series of reasons. The biggest step that helped control noise was to lower the tip speed, as this is the most significant parameter affecting it. In addition, *tonal* noise coming mainly from the mechanical parts has been reduced with the proper insulation of the nacelle [1, 2].

In most cases, simple or more sophisticated prediction models, such as the ones included in most commercial packages, in the planning stage are enough to ensure that a wind farm will not be a source of annoyance. However there have been cases that, for one reason or another, these predictions fail, leading to complaints. No prediction model is perfect and as models fail in the power generation predictions, they can easily fail in the noise prediction too.

In many cases, this failure has to do with bad siting or propagation effects that have not been taken into account (e.g. see [3]). Propagation of sound is a complex phenomenon, depending on atmospheric conditions, terrain type, reflections, refractions and so on: special atmospheric conditions or special landscape might propagate noise much longer than expected. Under certain conditions even off-shore farms could be heard km away in the shore as a result of multiple reflections on the sea surface in a downward refracting atmosphere. But also cases of wind turbines generating more noise than they should have been recorded, while the low-frequency and vibration problems have not been properly addressed.

In order to eliminate such problems more effort has to be put into continuously improving the noise performance of our wind turbines, especially if this can be achieved at low or no cost: a less noisy wind turbine will always be heard less than a more noisy wind turbine in any environment and conditions. In addition, quieter wind turbines could come even closer to dwellings solving space problems. It is therefore imperative to better understand the mechanisms behind wind turbine noise and thus reduce or eliminate it. Accurate noise generation models can help in optimizing wind turbines in this direction.

Noise from wind turbines has been studied before. Recently, it has even developed to an independent field needing its own conferences: the first conference on wind turbine noise took place in October 2005 in Berlin with a follow-up scheduled for 2007 in Lyon [4].

In the field of noise modeling, several models have been proposed through the times (e.g. [5, 6, 7]), ranging from very simplistic ones to complex CFD

---

solvers [8] that can however not be applied in practical means. For reasons of speed and accuracy, semi-empirical models are the most commonly used.

Some very important experimental results on airfoil self-noise with direct application to wind turbine noise were produced by Brooks, Pope and Marcolini, based on wind tunnel experiments on NACA0012 airfoils [9].

Wei Jun Zhu, in his master thesis in DTU, used the scaling laws given in [9], together with a turbulence inflow model proposed by Amiet [10] to develop a noise prediction model for wind turbines [11, 12]. The same functions have been used by others for similar modeling (see e.g. Fuglsang and Madsen [13] and Moriarty and Migliore [14]), their popularity demonstrating that they are probably the best in the market. What however makes the model by [11, 12] exceptional was the initiative to tackle these functions' main drawback, namely that they have been deduced for a specific, symmetric airfoil which is not used in modern wind turbines. This was done by calculating and storing the boundary layer thickness for different airfoils at different situations. In addition, many other features were implemented in the model, such as the influence of the tower and its geometry, the yaw, tilt and cone angles and the blade mass distribution.

The model was tested successfully against a Bonus 300 kW wind turbine and was used in a parametric study yielding many useful and interesting results.

This thesis is in many senses a continuation of [11, 12]. Its main aims are to further develop this model, to check it extensively against measurement data and to couple it with an optimization tool in order to optimize, not only a wind turbine's operational parameters, but also the wind turbine blade itself with respect to noise.

In chapter 2, a short description of the noise prediction model is given, both a summary of past work and also current developments. Chapter 3, presents the extensive noise measurement campaign at Høvsøre, while in chapter 4 we compare measurements and simulation results for a SIEMENS SWT-2.3-92 wind turbine. In chapter 5 the model is coupled to an optimization tool and used for optimizing the existing wind turbine's operational settings but also the wind turbine blade itself. Chapter 6 summarizes the main results.

Due to the confidential nature of the data this project was based on, many of the graphs appear in this report *normalized* (i.e. with non-dimensional or modified axes). The normalization is different for each graph. The original graphs can be obtained with permission and direct contact of SIEMENS WIND POWER A/S.

# Chapter 2

## The Noise Prediction Model

### 2.1 Summary of past work

In the noise prediction model by [11, 12], the airfoil *self-noise* noise modeling is based on the functions given by Brooks et al. [9]. These functions stem from wind tunnel experiments performed on NACA0012 airfoils. In total, *five* airfoil self-noise mechanisms were identified and studied separately:

1. the *Turbulent Boundary Layer Trailing Edge* noise
2. the *Separation-Stall* noise
3. the *Laminar Boundary Layer Vortex Shedding* noise
4. the *Tip Vortex Formation* noise and
5. the *Trailing Edge Bluntness Vortex Shedding* noise

Since the first two mechanisms were combined into one formula<sup>1</sup>, altogether four scaling laws were proposed, yielding the sound pressure level at the observer position as a function of frequency for the 1/3 octave band spectrum. It is remarkable that the scaling laws for all the mechanisms are of similar form:

$$SPL_i = 10 \log\left(\frac{\delta_i M^i L \bar{D}_h}{r^2}\right) + F_i(St) + G_i(Re) \quad (2.1)$$

---

<sup>1</sup>However no information is lost. In fact, the first equation consists of 3 terms: noise calculated for the *pressure* and the *suction* side of the airfoil at *zero angle of attack* and a component for noise at *non-zero angle of attack*. So the separation-stall noise can still be studied separately.

where  $\delta_i$  is a BL displacement thickness,  $M$  is the *Mach number* on a power  $i$ , depending on the particular noise mechanism  $i$ ,  $L$  is the airfoil section semi-span,  $\bar{D}_h$  is a sound directivity function and  $r$  is the distance to the observer. The additional terms  $F_i(St)$  and  $G_i(Re)$  are functions of the *Strouhal number*  $St = f\delta^*/U$  and the Reynolds number  $Re$ . The nature of dependency is different for each noise mechanism but it is still impressive that the 4 formulas look so much alike.

All the above mechanisms were termed as *airfoil self-noise* because they are a result of the interaction of the boundary layer of the airfoil with its trailing edge.

However, *turbulence inflow noise* is different: it is the result of the interaction of the existing turbulence in the wind with the leading edge of the airfoil. A prediction equation based on Amiet [10] has been implemented in the model:

$$L_p = 10 \log(\rho_0^2 c_0^2 l \frac{\Delta L}{r^2} M^3 I^2 \hat{k}^3 (1 + \hat{k}^2)^{-7/3}) + 58.4 + 10 \log(\frac{K_c}{1 + K_c}) \quad (2.2)$$

where  $l$  is turbulence length scale,  $I$  is the turbulence intensity,  $\rho_0$  is the density,  $c_0$  the speed of sound,  $\Delta L$  is the blade segment semi-span,  $\hat{k}$  is corrected wave length and  $K_c$  is a low frequency correction.

Reducing to the basics, we can state that in order to predict the noise spectrum at a *given observer position*, for a *given airfoil* we need to know the important following quantities:

- the boundary layer thickness  $\delta^*$  at the trailing edge of the airfoil
- the wind speed coming into  $M$  and  $Re$  and defined relatively to the airfoil by the angle of attack

Other parameters that influence the result, are the state of the boundary layer transition (forced or natural, leading to tripped or untripped flow) and all parameters that are input to the *turbulence inflow* noise computation, such as the the *turbulence length scale* and the *turbulence intensity*, finally reducing to the knowledge of the height from the ground  $z$  and the roughness length  $z_o$ .

It is not the purpose of this thesis to go into details describing the theory behind [9] and [10], since this has been done extensively in [11]. For details on the nature of each noise mechanism, the reader is advised in these references.

### 2.1.1 The Boundary Layer Thickness Database

It was just mentioned that an important parameter for the calculation of airfoil self-noise is the boundary layer thickness at the trailing edge. This is calculated by use of the program XFOIL [15].

Instead of a dynamic interaction of the code, which runs in MATLAB environment, with XFOIL, a database was constructed where the boundary layer thickness was stored for different values of Reynolds number and angles of attack. Then  $\delta^*$  is calculated by interpolation. Wei Jun Zhu, populated this database with 11 different airfoil types.

In fact *two* databases exist, corresponding to tripped and untripped flow, as these result in different boundary layer thicknesses and therefore at different noise levels. These two different situations of boundary layer transition were modeled in XFOIL by changing the BL parameter  $N_{crit}$ , giving the inflow turbulence level, from value  $N = 9$  for untripped to  $N = 4$  for tripped flow. The corresponding turbulence levels are 0.070% and 0.563% respectively.

For the needs of the current project, the database was expanded to include 5 more airfoil types, which are the ones used in the B45 blade. In figure 2.1, the stored BL displacement thickness is displayed for the FFAW3241 airfoil.

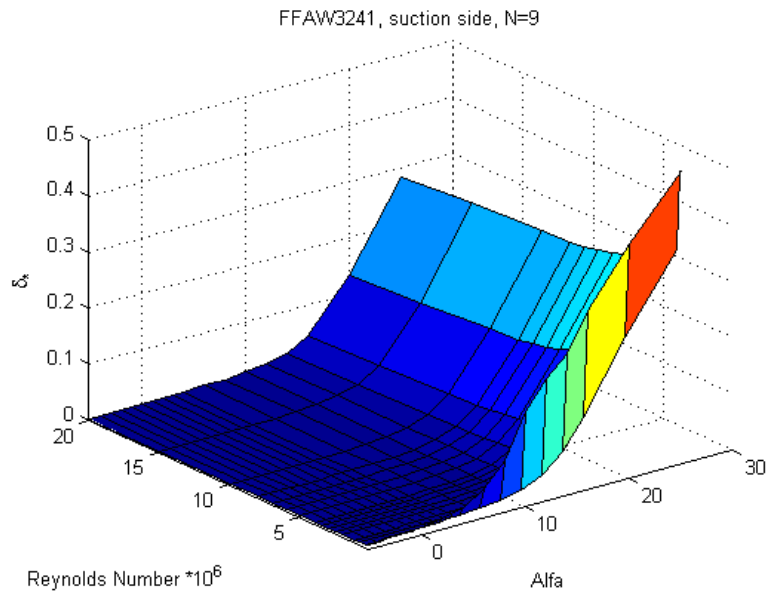


Figure 2.1: Boundary layer displacement thickness at the trailing edge of FFAW3241 as a function of the Reynolds number and the angle of attack

## 2.2 The code BEM-NOISE

A disadvantage of the model presented in [11, 12] was that the relative velocities seen by the blade elements had to be computed separately by a BEM code. The values were saved in a file and given as an input to the code. This prevented the code from running dynamically and made multiple runs certainly a difficult issue. Therefore, the first major modification that was required in order to make this code exploitable for optimization purposes was to combine the noise prediction model with a BEM code so that it would give both estimated noise and power production levels at one run. Besides the optimization oriented advantages, this also ensures the biggest possible accuracy and error minimization concerning the crucial relative velocities.

This gave rise to the code BEM-NOISE which works roughly as seen in the flowchart seen in figure 2.2.

Except the traditional input to a BEM code (chord, twist, relative thickness and airfoil type distributions along the blade), a series of additional input is required for the model to run. The most important of these are:

- The observer position relative to the wind turbine and all the necessary quantities for coordinate system transformations (including yaw angle, tilt angle, etc)
- The bluntness of the blade at the trailing edge and the trailing edge angle
- Whether the flow is tripped or untripped
- All the necessary quantities to compute turbulence properties, such as the wind shear factor  $\gamma$  or the roughness length  $z_o$ .

The user specifies for which combination of wind speeds, rotational velocities and pitch angles the calculations need to be made and the code proceeds more or less as a traditional BEM code. At least until the point where the relative velocities  $V_{rel}$  seen by the blade elements are calculated. There, the function *NOISE* is called, which makes a table look up at the BL thickness database and calculates the Sound Pressure Level  $L_p$  at the *observer position* due to the particular blade element for each noise mechanism *separately*, with the help of the functions provided by [9, 10]. Finally, the sound pressure levels are added for all the elements and all the blades, converted to sound *power* levels  $L_w$ , referring to the hub of the wind turbine, and saved for plotting, processing, etc. Of course all traditional BEM output are also available.

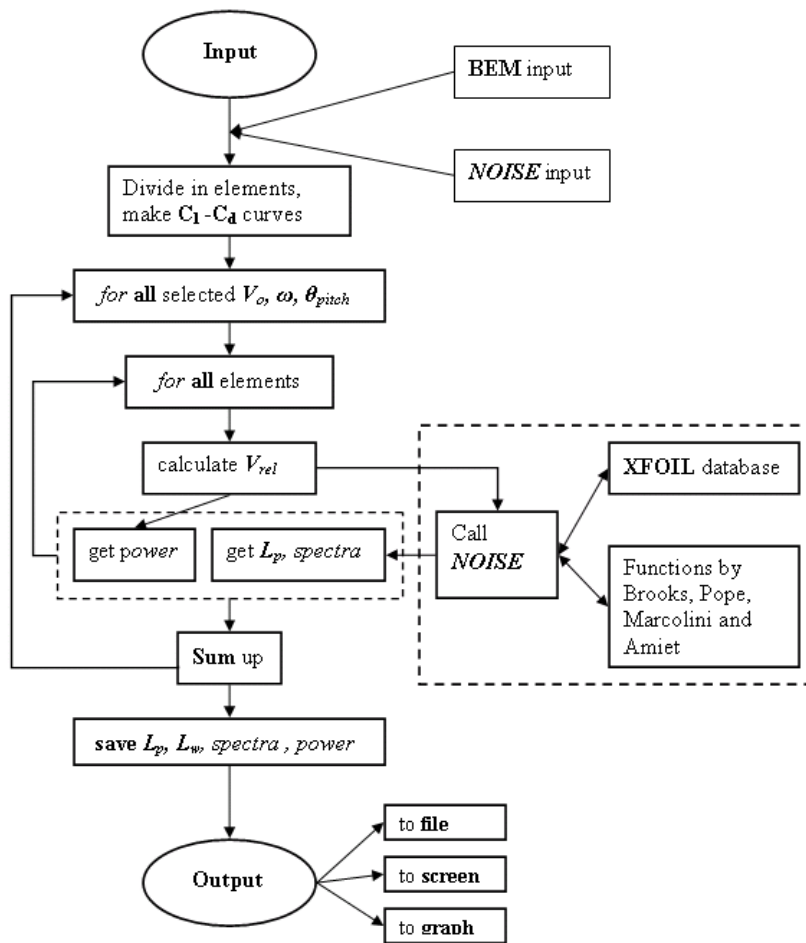


Figure 2.2: Flowchart of the code BEM-NOISE

Figure 2.3 shows a power production vs. noise generation graph for the SIEMENS SWT-2.3-92, generated by BEM-NOISE. Of course, over rated power, there are more than one corresponding  $L_w$  due to the increasing wind speed and the changing pitch angle.

It should be pointed out that this is only a general outline of the code which is more flexible than this: also individual mechanisms at individual parts of the blade can be studied, while it is also possible to couple it to an optimization routine.

Finally, it should be mentioned that for each particular set of parameters a maximum runtime of a few seconds is required in order to achieve convergence (dependent on the number of blade element segments), so one of the major advantages of this prediction model together with its accuracy is its speed.

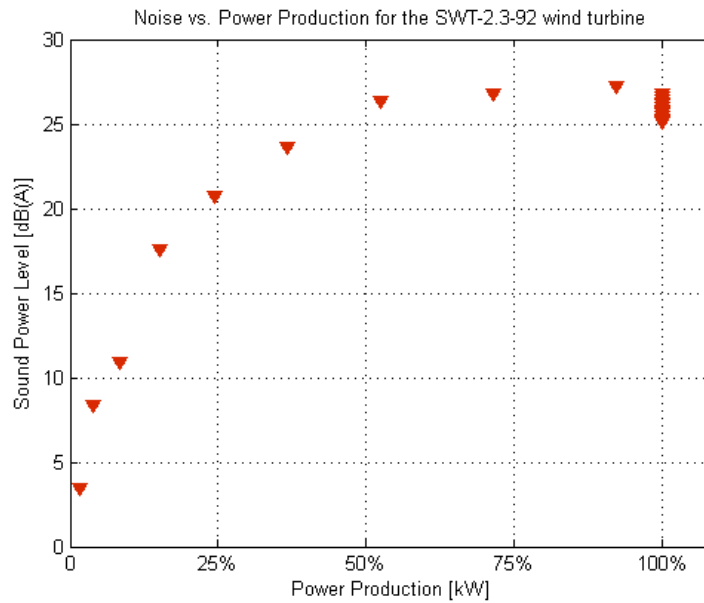


Figure 2.3: Noise vs. power production for the SWT-2.3-92 wind turbine

# Chapter 3

## Noise Measurements Campaign Description

The noise measurements were performed on a SWT-2.3-92 wind turbine at the Risø National Laboratory Test Site for large wind turbines at Høvsøre. The project took place under the supervision of Ejler Kristensen from SIEMENS WIND POWER A/S. Two days of measuring resulted in ca. 11 hours of data.

Our aim was to be able to measure at a large variety of settings: if the reader pictures a two-dimensional matrix with pitch angle and rpm as the two dimensions, and each element of the matrix being the  $L_p$  in the corresponding coordinates, the purpose of our campaign was to fill in as many elements of this matrix as possible.

### 3.1 Area Description

The test site at Høvsøre is by the western coast of Jylland where the strongest winds in Denmark occur. The terrain is flat, no major obstacles exist and the sea is situated to the west. There are 5 test positions and the SWT-2.3-92 was ideally situated for noise measurements at the end of the row to the south. The terrain is covered with grass.

As dictated by the corresponding IEC standard for measuring wind turbine noise [16], a list of the major noise sources in the area needs to be provided. These for our case were:

1. The sea: indeed when the wind speed is high enough, the sound from the generated waves can become audible at low frequencies increasing the background noise.



Figure 3.1: A picture of the Høvsøre test site. The SWT-2.3-92 was positioned in the last test position

2. The birds: the singing of the birds is a source of concern, especially because of its random nature. Their influence was particularly visible in the frequencies between 2000 and 7000 Hz and the measurements had to be filtered for their presence.
3. The other wind turbines. In our case this was not a problem since the two closest wind turbines (as well as the furthest) were out of operation the whole interval, due to maintenance work. The fourth wind turbine, which was operational for part of our campaign, is too far to influence our measurements. In fact it would have been enough if just the closest wind turbine was shut down, as was the case.
4. The presence of a farmer harvesting his neighboring fields by use of tractors. This would definitely influence our measurements in a non predictable way and therefore no measurements were performed until he packed and left!

It is obvious that despite the above sources, in total, the area is very quiet since there are no major roads, air traffic or such noise sources. The environment is as close to ideal for noise measurements.

## 3.2 Wind Turbine Description

The SIEMENS SWT-2.3-92 is a variable speed, pitch regulated machine with the following characteristics:

- Rated Power: 2300 kW
- Cut-in Wind Speed: 3 m/sec
- Cut-out Wind Speed: 25 m/sec
- Variable rotational speed, depending on the wind speed
- Variable pitch angle to maintain rated power

The tower height of the particular machine at Høvsøre is 80m.

## 3.3 Meteorological Conditions

The wind speeds these two days were not very high making it possible to take good measurements. If the wind speed is *too* high, the wind turbine noise gets masked from the background noise, such as leaves, trees, waves, etc. During our campaign, we captured enough 10sec averages in most wind speeds between 3 and 12 m/sec. However, the wind conditions were not identical during the different measurement series: in the first day (from now on: *Day 1*) we had a mean wind speed of  $8.5 \pm 1.7$  (std). In the second day however, we started in the morning (from now on: *Day 2,s1* -standing for series 1) with much lower wind speeds (i.e.  $5.6 \pm 1.4$ ) while the wind picked up later in the afternoon (from now on: *Day 2,s2*) giving  $9.8 \pm 1.9$ . As a result we had a lack of measurements at high wind speeds in Day 2,s1, while we had a lack of measurements at low wind speeds in in Day 2,s2.

## 3.4 Instrumentation

All microphones and instrumentation used were by Brüel and Kjær as was also the software PULSE [17] used to collect, process and plot simultaneously the instantaneous data coming in from the microphones. In addition, data from the wind turbine, such as wind speed, power production, pitch and yaw reference and shaft and generator rotational speed, were also logged in the data collector and recorded in parallel with the noise measurements. The result was text files containing 10sec averages for all the above quantities and 1/3 and 1/12 octave spectra.

## 3.5 Measurement Location

Measurements were performed simultaneously at 4 different locations:

1. at 100 m downwind,
2. at 150 m downwind,
3. at 20 m on the rotor plane and
4. at 150 m on the rotor plane

where all distances were measured from the tower bottom and the rotor plane measurements were taken at the blade descending side. However, it should be stressed that the control system of the wind turbine continuously yaws the wind turbine into the instantaneous wind direction and therefore the rotor plane does *not* remain constant. It is rather the *initial* positioning of the microphone that was on the rotorplane. There will be more about this in 4.2.

## 3.6 Procedure

The following procedure was followed during measurements. Day 1 was entirely dedicated in varying the rotational speed, while Day 2 was dedicated into pitch variation. More specifically:

1. During Day 1, the rotational speed of the wind turbine was varied stepwise between 10 and 14 rpm at 20min steps with intermediate stops to capture the background noise.
2. During Day 2,s1, the pitch was varied systematically from +10 to -2 deg at low and medium rpm (10 and 13 rpm). In order to capture as many different combinations as possible, 5min averages were taken at each step.
3. During Day 2,s2 the same procedure was followed as in Day 2,s1 only at very high rotational speed (17rpm - which is actually more than the maximum of the SWT-2.3-92 normal operational conditions)

## 3.7 Data Processing

The 10sec averages which were given as an output from PULSE had to be corrected for 3 different effects:

1. the background noise
2. the bird noise and
3. the measurement board

This was done in MATLAB and according to the procedures suggested by the IEC standard [16]. In brief, in order to remove the background, the data is binned in integer wind speeds. First the background noise is calculated for each velocity bin and subsequently it is subtracted from the total noise as follows:

$$L_p = 10 \cdot \log(10^{0.1L_{total}} - 10^{0.1L_{background}}) \quad (3.1)$$

This is done both for the broadband noise and the spectra, showing the distribution of the sound pressure per frequency.

Finally, the sound *pressure* level  $L_p$ , measured at the microphone, is converted to sound *power* level  $L_w$  (which is a property of the source) at a distance  $R_1$  from the microphone:

$$L_w = L_p - 6 + 10 \cdot \log\left(\frac{4\pi R_1^2}{S_o}\right) \quad (3.2)$$

Here  $R_1$  refers to the hub of the wind turbine, i.e. we approximate the wind turbine as a point source concentrated at the hub. The reference surface  $S_o = 1m^2$ .

The correction applied for the measurement board is *also* included in equation 3.2: it is simply the  $-6dB$  term that corrects for a fully reflective surface<sup>1</sup>.

In figures 3.2, 3.4 and 3.4, we have plotted the background spectra for the three obtained time series. We should point out that the background noise at Day 2,s1 for 5 and 6 m/sec turned up unreasonably high (even much higher than for 7 m/sec !). For this reason, we considered using the corresponding spectra from Day 1, instead. The highest noise content in the low frequencies

<sup>1</sup>a doubling of the pressure corresponds to a 6dB increase in the dB scale

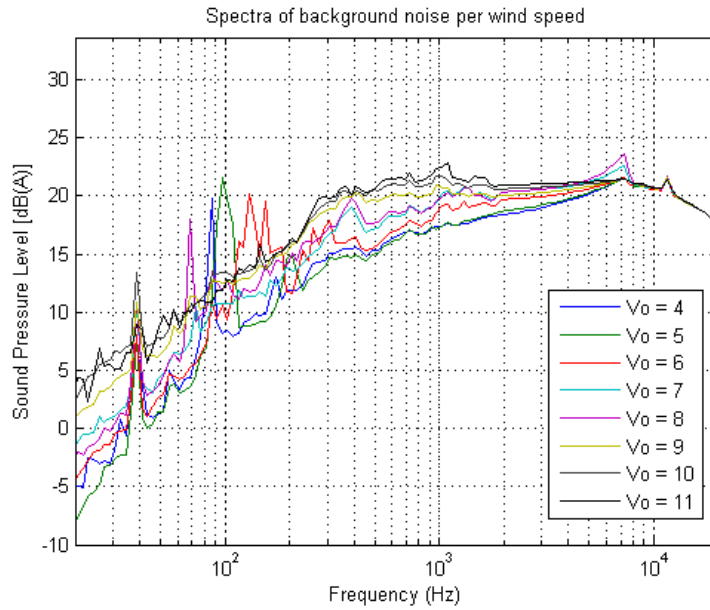


Figure 3.2: Background spectra for Day 1. All wind speeds from 3 to 11 m/sec were captured

in day 2, series 2 is due to the presence of the waves as explained earlier, which appeared in the afternoon of Day 2.

In figure 3.2 the background spectra per wind speed are displayed for day 1 and day 2, series 2, so that all wind speeds are covered.

As far as bird noise is concerned, this was visible in frequencies between 2000 and 7000 Hz (figure 3.5). The data had to be filtered for this effect to be removed.

Notice also that all spectra converge to the same value over 10 kHz. This is equal to the background noise and it means that no noise is produced above these frequencies

The result of our measurement campaign can be summarized in figure 3.6 where all our measurement points have been plotted as a function of  $\omega$  and  $\vartheta_{pitch}$  and with the  $L_w$  in the z-axis.

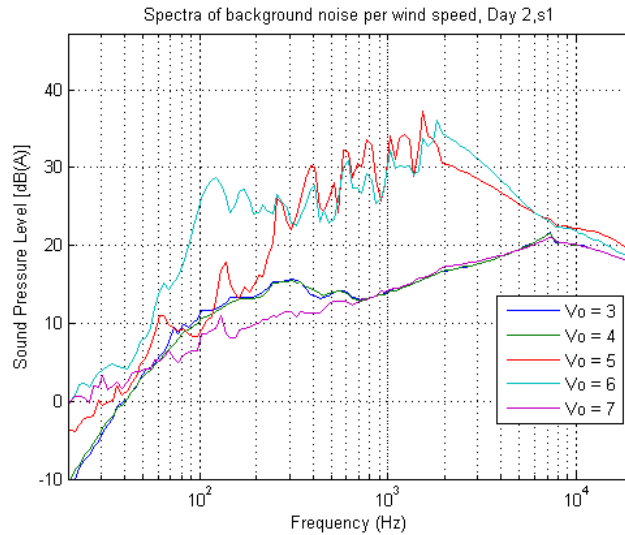


Figure 3.3: Background spectra for Day 2,s1 (morning). Few (low) wind speeds were captured. Notice that the background spectra for 5 and 6 m/sec are too high. There is almost certainly something wrong with them. The corresponding spectra from Day 1 were used instead

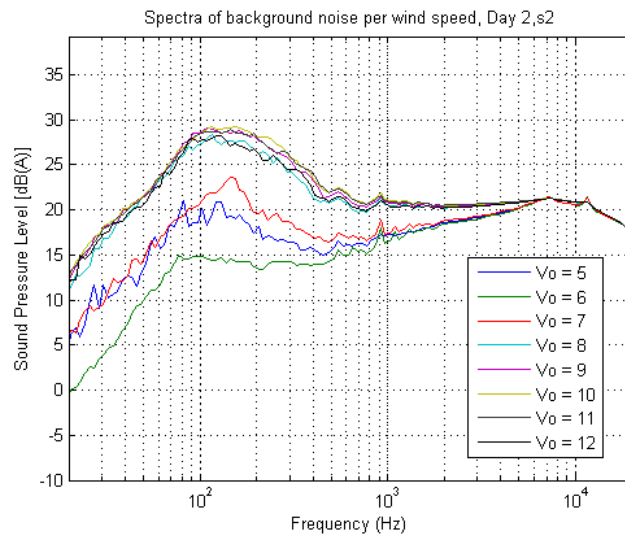


Figure 3.4: Background spectra for Day 2,s2 (afternoon). Most wind speeds were captured. The increased low frequency content of the spectra is attributed to the sea waves

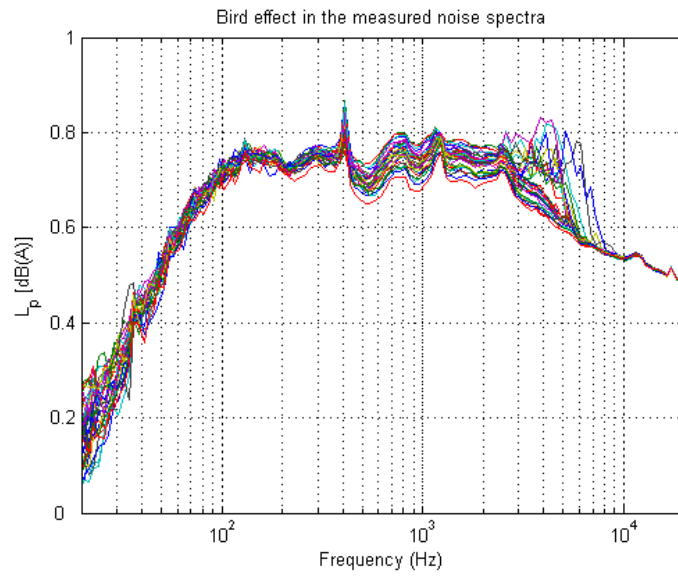


Figure 3.5: Thirty raw consecutive noise spectra from a (random) 5 minute interval are displayed. In some of them (but not all), peaks appear between 2 and 7 kHz. This is the effect of (random) bird singing.

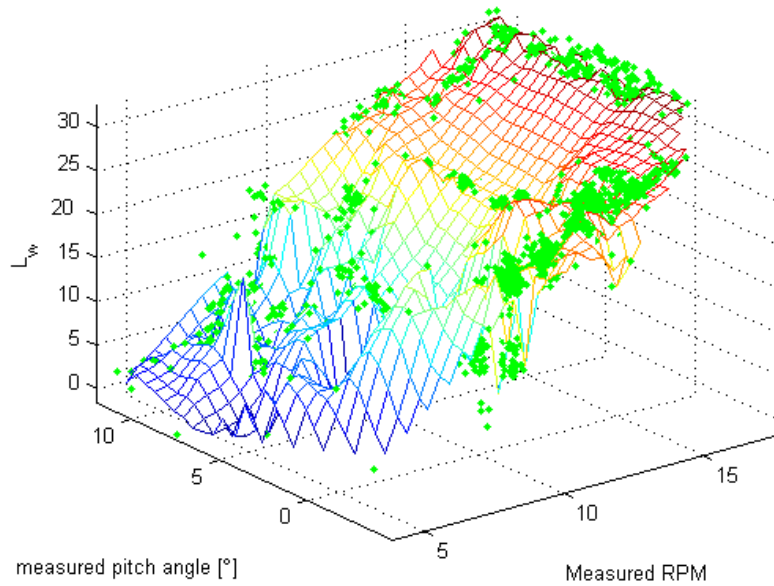


Figure 3.6: The results of our measurement campaign summarized in one graph:  $L_w$  as function of RPM and pitch angle. The green points are all the obtained data points

# Chapter 4

## Results

Almost all measurement results that are presented in this thesis, with the exception of section 4.2, come from the microphone that was positioned 100m downwind. This had the best noise-to-signal ratio. In addition, all simulation results, unless otherwise stated, refer to this same distance.

Some preliminary conclusions can be deduced from an elementary study of the measured time series. These are displayed in figures 4.1, 4.2 and 4.3 for the quantities  $L_p$ ,  $\omega$  and  $\theta_{pitch}$  and for measurements taken in Day 1, Day 2,s1 and Day 2,s2, respectively. The stepwise variations in  $\omega$  (Day 1) and  $\theta_{pitch}$  (Day 2) and their effect on  $L_p$  can be clearly seen. We notice however that the Day 2,s1  $L_p$  series demonstrates a much noisier behavior, at least during the first hour.

The study of the correlation coefficients can be seen in table 4.1, for each measurement series separately.

It can easily be seen that the strongest correlated quantities are  $L_p$  with  $\omega$  (correlation coefficient around 85-90%), while the other time series are more loosely correlated. This confirms our feeling that  $\omega$  is the most crucial parameter affecting noise. The fact that the correlation coefficient between  $L_p$  and pitch is negative, indicates that an increase in one quantity is related to a decrease in the other. Wind speed is less important, but still plays a role as we will see later. We observe that the correlation coefficients for Day 2,s1 (morning) series behave slightly differently: despite the fact that the varied quantity is the pitch angle, the correlation is very loose, while the wind speed's importance has increased. If we remove the noisy part however, the correlation coefficients become 0.9, -0.7 and 0.13 respectively, resembling much more the other time series characteristics.

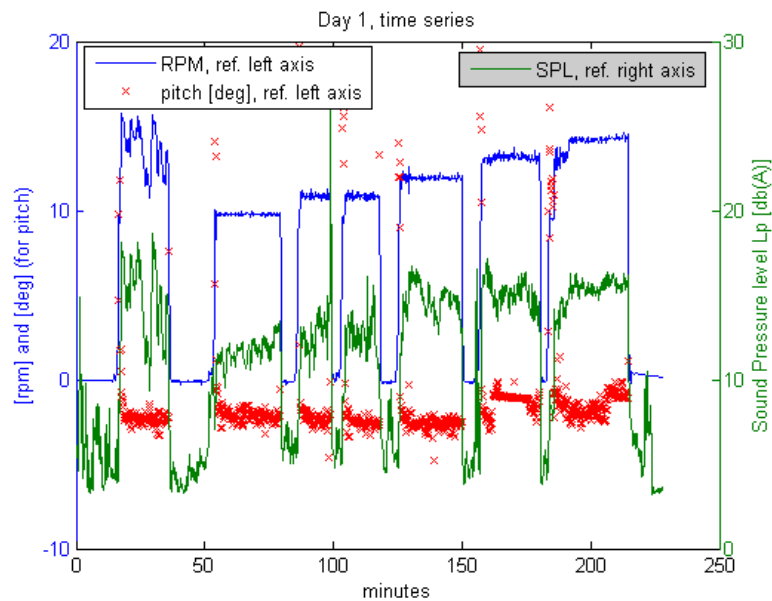


Figure 4.1: Time series from Day 1 measurements. In blue is the rotational velocity in rpm and in red the pitch angle in degrees (read from left axis). In green the (raw) sound pressure level (read from right axis)

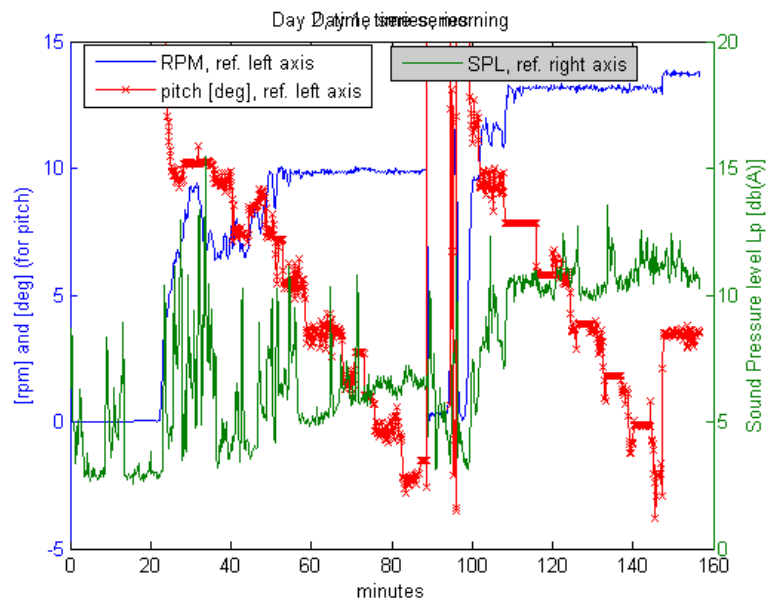


Figure 4.2: Time series from Day 2, s1 measurements. In blue is the rotational velocity in rpm and in red the pitch angle in degrees (read from the left axis). In green the (raw) sound pressure level (read from the right axis).

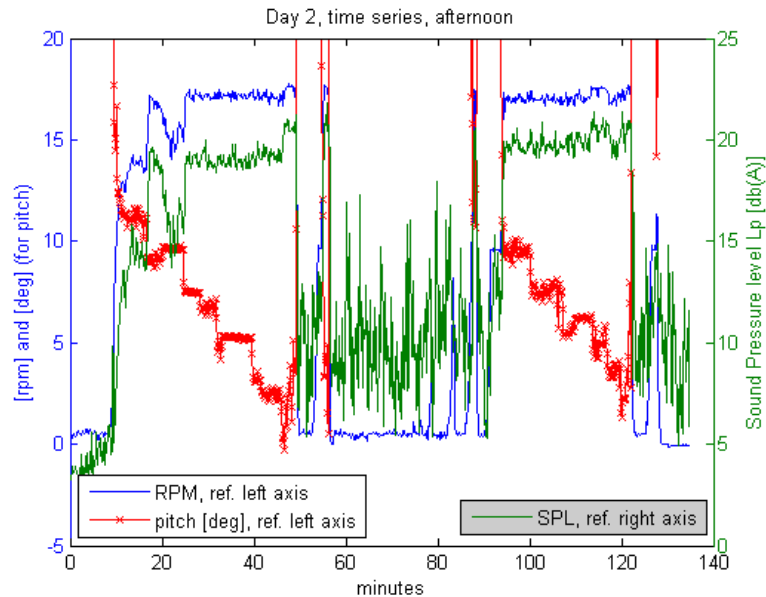


Figure 4.3: Time series from Day 2,s2 measurements. In blue is the rotational velocity in rpm and in red the pitch angle in degrees (read from the left axis). In green the (raw) sound pressure level (read from the right axis)

Corr. Coeff.	Day 1	Day 2,s1	Day 2,s1 B	Day 2,s2
$L_w$ , RPM	0.8669	0.9025	0.9003	0.8983
$L_w$ , pitch	-0.5817	-0.2826	-0.7087	-0.7049
$L_w$ , $V_o$	0.1894	0.5928	0.1299	0.1372

Table 4.1: Correlation coefficient between the time series,  $L_w$ , rpm, pitch and  $V_o$ . Under Day 2,s1 B, only the second part of this time series has been examined (i.e. the noisy first hour has been removed)

## 4.1 Extensive Validation

Wei Jun Zhu, validated his prediction model against a Bonus Combi 300 kW turbine and the model proved to be doing fairly well [11, 12]. However, due to the lack of experimental data, the validation was restricted to one noise spectrum obtained at one wind speed. It says a lot about the availability of experimental data in this field that Fuglsang and Madsen [13], validated their model against the same spectrum, referred in [18] back in 1993.

It is therefore mandatory to further validate this model against a series of parameters as wind speed, rotational velocity and pitch angle in both broadband noise and noise spectra. The reasons are that the model might perform excellent under certain conditions and poorly under others. All these factors are very important to know, since the model is going to be used for optimization. In addition, it is not for granted that because the model performed well against the Combi 300 kW, this is also going to be the case for the SWT-2.3-92 wind turbine. There are huge differences between the two turbines, the one being stall regulated and the other variable speed and pitch regulated to name but a few. But without doubt the most important difference between the two turbines is their size: the rotor of the Combi 300 kW is only 30m of diameter while the one from the SWT-2.3-92 is three times as big!

The detailed data obtained at Høvsøre offers the most excellent occasion for such a task.

The first ambition for the model performance is that it at least captures the *trends* shown in the experimental data. It is believed that even in this case, it should be good enough to use for optimization purposes, since the relative differences in noise production, between two different settings, would remain unchanged.

In all comparisons, the result for tripped flow was used (see section 2.1.1) for simulations, because we believe it simulates best real life conditions. Due to dust, dirt and/or sea salt, the flow over a wind turbine blades airfoil will almost always be tripped.

### 4.1.1 Against Default Operational Settings

By *default settings*, it is meant, throughout this report, the wind turbine's default operational settings (i.e the rpm and pitch angle values that the wind turbine operates on, depending on the actual wind speed). It is very important that the model captures correctly the behavior of the wind turbine in its existing settings, because these settings are going to be our starting point for all optimizations performed in chapter 5. Because our campaign

purpose was exactly to *change* these settings and see how the wind turbine behaves, we obtained data for *normal operation* for a limited time only: the wind turbine operated in normal mode only for the first part of Day 1, and it is therefore against *this* data that we have to validate our model.

In figure 4.4, we show the computed 'Noise Curve' of the SWT-2.3-92 wind turbine<sup>1</sup>, together with all the measured points and a best fit through those points including a double standard deviation interval, giving a 95% confidence.

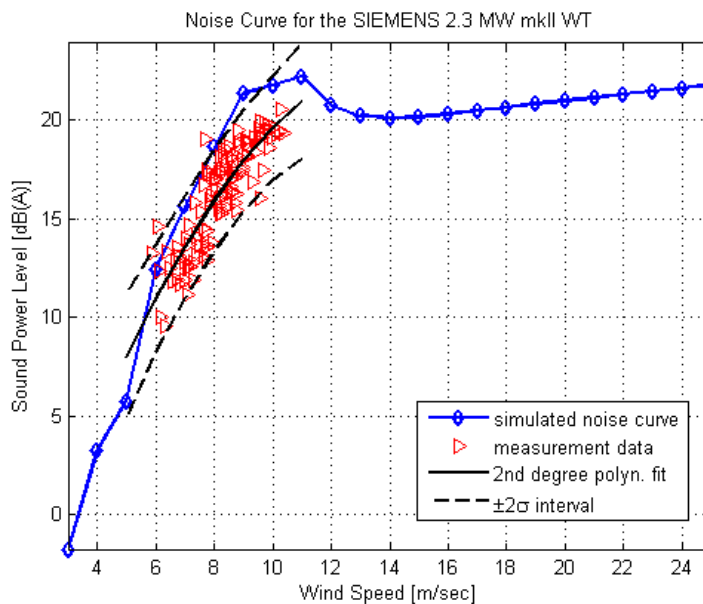


Figure 4.4: The noise curve for the SIEMENS SWT-2.3-92 operating at its default settings, as computed by BEM-NOISE. For wind speeds between 6-10 m/sec there are also measurements and the agreement is good

We observe that the simulation slightly overshoots the measurements, staying however within the 95% confidence interval, while it certainly captures the right trend.

### 4.1.2 Against Rotational Velocity

It has been explained that rotational velocity is the most crucial parameter for noise production. It is therefore vital that the model shows the right behavior with the  $\omega$  variations. It was in Day 1, that we performed rpm

<sup>1</sup>something like the power curve, with the difference that instead of power we plot the  $L_w$  against the wind speed

variations and it is therefore with *this* data that we should compare our simulation results.

In figure 4.5, we have plotted our simulated result, against all measurement points. A best fit to the measurements has been added together with an 95% confidence interval. The simulation curve is for the mean wind speed at this time. The agreement is excellent!

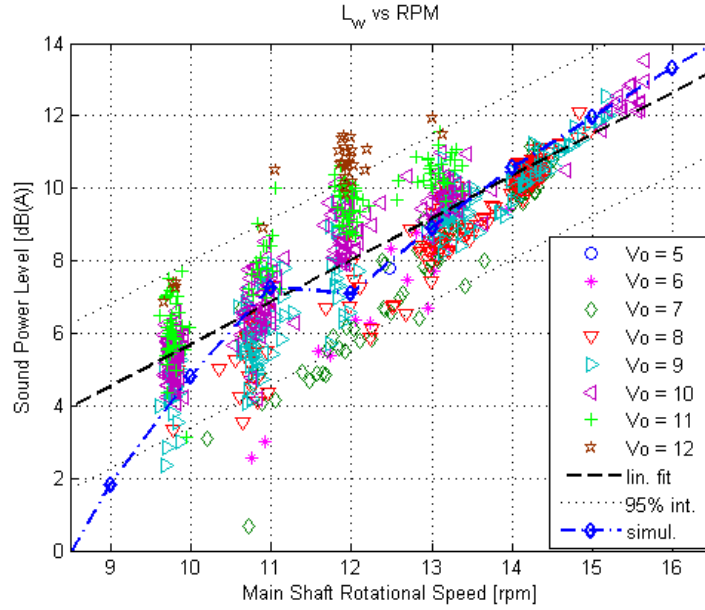


Figure 4.5: Simulation against measurement for the rpm-noise dependency

We observe that both simulations and measurements have a clear *linear* behavior (within this interval), which confirms the high correlation coefficient shown in table 4.1 and the feeling we had about the importance of  $\omega$ .

A regression analysis gives the following relation between  $L_w$  and  $\omega$ :

$$L_w = 1.16 \cdot \omega + 86.12 \quad (4.1)$$

where  $L_w$  is given in dB(A) and  $\omega$  in rpm. This equation can be used for a (rough) noise prediction when  $\omega$  is changed. However, it should be remembered that it is only valid for the *default* pitch angle (opti-pitch) and that it is probably not valid at much lower rpm.

The measurement points have also been grouped in different wind speeds (different colors). It can be observed that there is a clear tendency of points with higher wind speeds to lie above points with lower wind speeds at the same rpm: while the rpm is the prime factor that determines noise, the wind

speed also plays a minor role. The pitch angle remained almost constant throughout Day 1.

### 4.1.3 Against Pitch Angle

In order to study the pitch dependency of the wind turbine noise, I present in this section three graphs, showing the noise dependency on the pitch angle at high, medium and low rpm (17, 13 and 10 rpm respectively). In all three graphs a best fit with a 95% confidence interval has been applied to the experimental data. All simulations were made for the mean wind speed at the time of the measurements.

#### High RPM

Since the pitch dependency is less strong than the rpm dependency, it was important to keep the rpm constant during these experiments. The measurements at Day 2,s2 were actually performed at an RPM that is outside the operational limits of the wind turbine (17 rpm), that is we tried to go a little on the noisy side!

We observe that the agreement between simulations and measurements was again excellent. The noise clearly increases when we pitch toward stall, and this is due to the increasing importance of the boundary layer *separation noise mechanism*, as the angles of attack become higher.

#### Medium and Low RPM

In contrast to the *high* rpm measurements, the *medium* and *low* rpm (13 and 10 rpm respectively), were taken in the morning of Day 2 (Day2,s1). Unfortunately, this time the simulations do not show as good accordance with the measurements and they tend to overshoot them by approximately 3 and 6 dB(A) respectively. However the general trend is captured (i.e. the turbine becoming noisier as we approach the stall region) and this is good.

The reason for this offset might be due to a bias in the code and, in this case, it has to be corrected. This could be done by forcing a -3 and -6 dB(A) *penalty* for these rpm, while intermediate values could be calculated by interpolation. This however would influence the good performance of the model in other fields.

It should be stressed however that the Day 2,s1 series has presented some abnormalities: the very noisy signal (at least in its first part, where also most background measurements were performed), the completely anomalous background (figure 3.3), which partly had to be replaced by the background

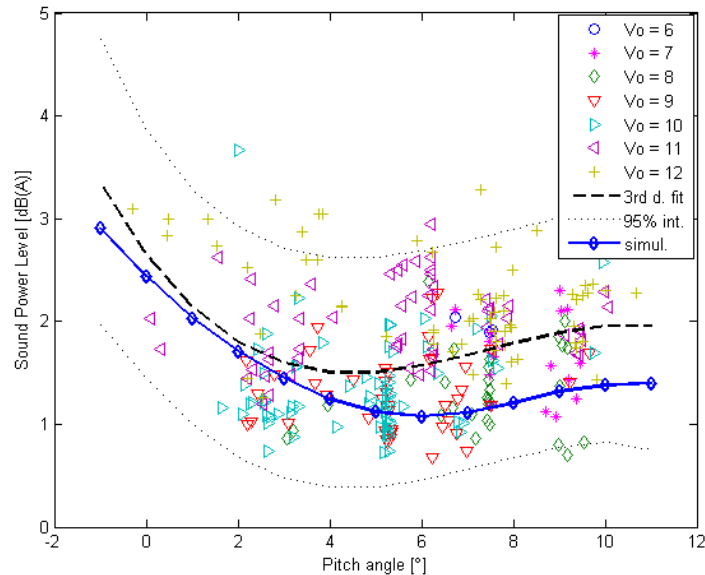


Figure 4.6: Simulation against measurement for the noise vs. pitch dependency at high -17- rpm

measurements from Day 1, which were more reliable, and the different correlation coefficients compared to the other two series (table 4.1), which were *corrected* after we cut the first part of the time series. However, in this case, even if we remove this part (corresponding to the low -10- rpm measurements), this does *not* solve the -3 dB(A) undershoot for the medium -13- rpm part of the series.

Nevertheless, these signs suggest that there might be something irregular with the Day 2,s1 measurements, although nothing came to our immediate notice while collecting the data. The biggest proof for this is an observed discrepancy between measurements *themselves* in Day 1 and Day 2,s1: during the morning of Day 2, the wind turbine operated at some common settings with Day 1, namely at 10 rpm *and* default pitch and 13 rpm *and* default pitch. It turns out that the measurements in Day 2,s1 were considerably quieter than the ones from Day 1, which should not be the case. Just the difference in wind speeds (maybe 3-4 m/sec) is not enough to explain a difference of 4 dB(A) in noise between two else wise equal measurements. It is therefore impossible for the simulations to comply with both the results from Day 1 and from Day 2,s1. All this, suggests that this time series should be treated with caution, and we believe that figures 4.7 and 4.8 do not provide enough evidence to rule out or severely modify our prediction model.

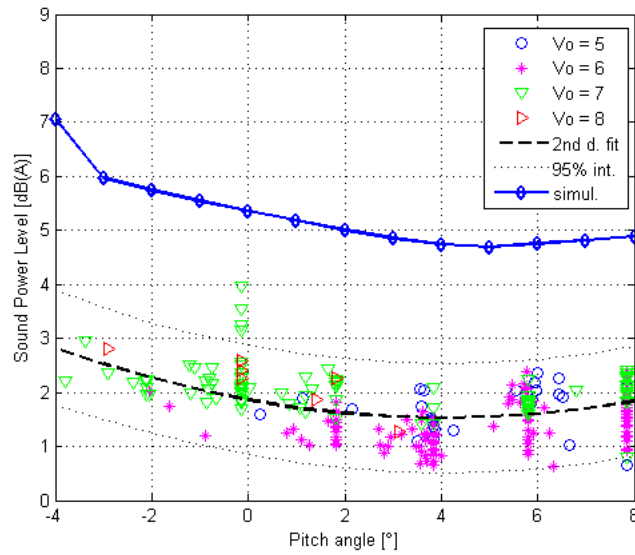


Figure 4.7: The noise-pitch dependency at medium -13- rpm. An overprediction of around 3 dBs is observed. However the simulation follows the correct trend

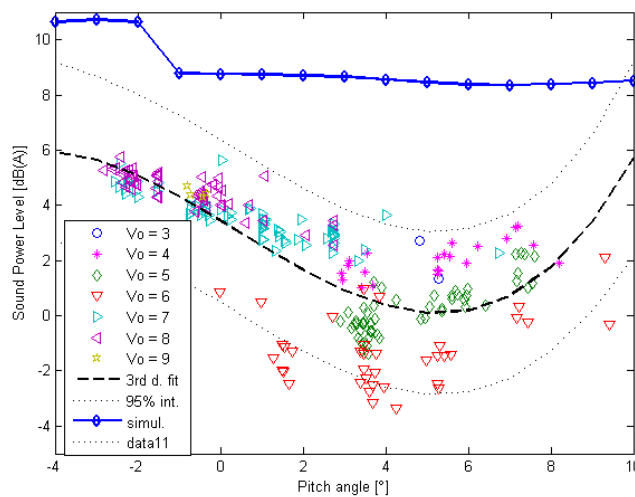


Figure 4.8: The noise-pitch dependency at low -10- rpm. An overprediction of around 6 dBs is observed!

Again, in all three pitch-figures, the measurement points have been sorted in different wind speed groups. For once more, we observe that points with common rpm and pitch angle are on average higher at higher wind speeds. This is again what was expected.

#### 4.1.4 Against Both

It is possible to create noise contours by interpolating between the measurement points in the  $(\omega, \vartheta_{pitch})$  space, in order to obtain knowledge of the noise levels in the areas where we did *not* perform measurements. These contours can be seen in figure 4.9.

It is also possible to generate the same contours by simulation (figure 4.10). Although the theoretical curves are naturally more smooth, the two figures resemble fairly each other to a good degree and present some common qualitative features. At high rpm's the contours are parallel to each other, while the stall region can clearly be seen in the theoretical contour plot: one can almost draw a straight line connecting the angles, where the noise contours turn and the turbine becomes noisier due to boundary layer separation noise.

Of course direct comparison is not possible because the experimental contours are for a diverse set of wind speeds, while the simulated contours displayed in figure 4.10 are for a single wind speed (10 m/sec).

#### 4.1.5 Against Spectra

All comparisons above were made for the sound power level  $L_w$  (one scalar quantity). In this section we compare 1/3 octave spectra measured in the field and computed by simulations for different operational settings.

The experimental spectra are the average of spectra of measurement points with similar parameters. For example, in figure 4.11, the experimental spectrum is the average of all the measurement points which had  $13.5 < \omega < 14.5$ ,  $-3 < \vartheta_{pitch} < -1$  and  $7 < Vo < 9$ . It was a prerequisite that at least 30 measurement points were averaged in order to get a good statistical sample. The simulation spectra were produced for the averaged settings (e.g. in case of figure 4.11:  $\omega = 14$ ,  $\vartheta_{pitch} = -2$  and  $Vo = 8$ ).

In general, the agreement between measurement and simulation varies from case to case ranging from good to bad, without being able to distinguish a pattern on when this happens. In the following figures we have displayed some (representative) examples.

It is important to observe the following: sometimes, we can obtain excellent agreement between simulation and measurements in the frequency range

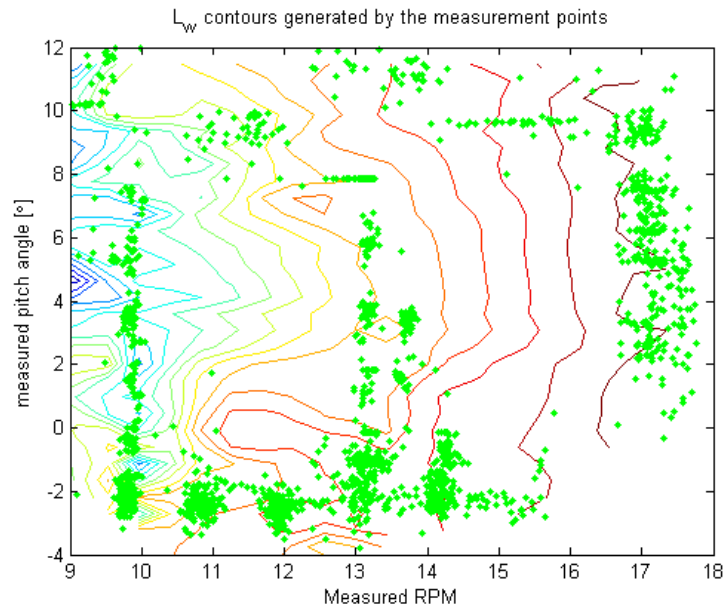


Figure 4.9: These contours were generated from the experimental data

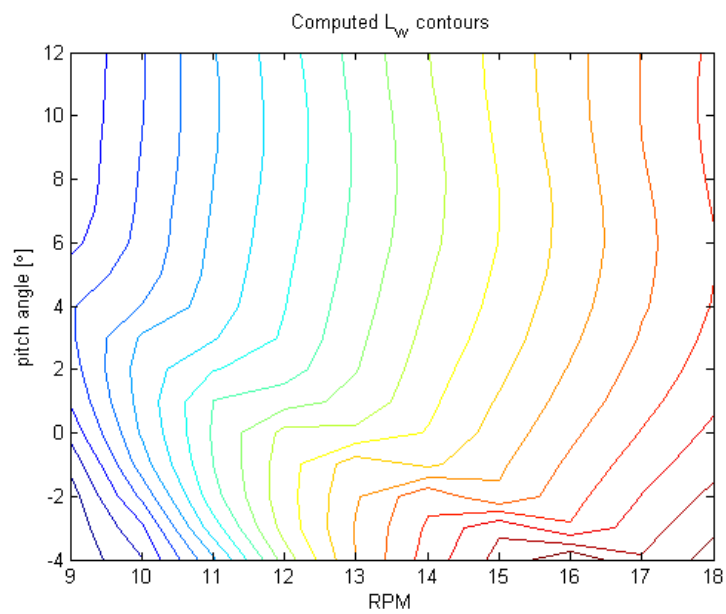


Figure 4.10: These noise contours are the result of simulation

up to 2000 Hz. Even when a perfect match fails, the simulation curves follow in general the behavior of the measured spectra in this interval.

The simulation however, systematically overpredicts the experiment for frequencies over 2000 Hz. Even a *peak* appears in an area where virtually nothing appears in measurements. This peak, as can be seen in figure 4.13, where all individual noise mechanisms are displayed, and further investigated in page 39, can be mainly attributed to the *Trailing Edge Bluntness* noise, which is responsible for this kind of *tonal* behavior. If this mechanism is removed from calculations, much better agreement is obtained. This might be a sign that the Bluntness mechanism prediction model is not that accurate and could be improved.

However the model should not be taken seriously for frequencies above 10000 Hz. It is obvious even from the pre-processed, *raw* data (figure 3.5) that the wind turbine does not generate absolutely any sound above this frequency. However the prediction model gives something. Probably these prediction equations do not give so good results at such high frequencies.

#### 4.1.6 Summary

We believe that our prediction model behaves quite well in most situations it has been tested against. A *slight* overprediction for the default operation (see figure 4.4) can probably be explained from the (simulated) excess of sound power in the high frequency spectrum. An important overprediction is also shown in figures 4.7 and 4.8, but we have good reasons to believe that it is the measurements that are responsible for this discrepancy. However, the trends versus the rpm and pitch variations are obeyed more or less well.

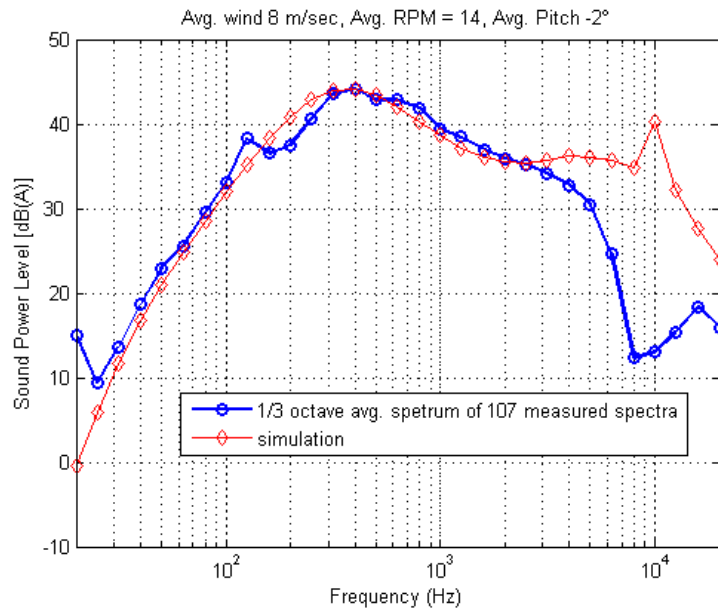


Figure 4.11: For these particular settings, excellent agreement is shown between simulated and (averaged) measured spectra. This is true for frequencies up to 3000 Hz.

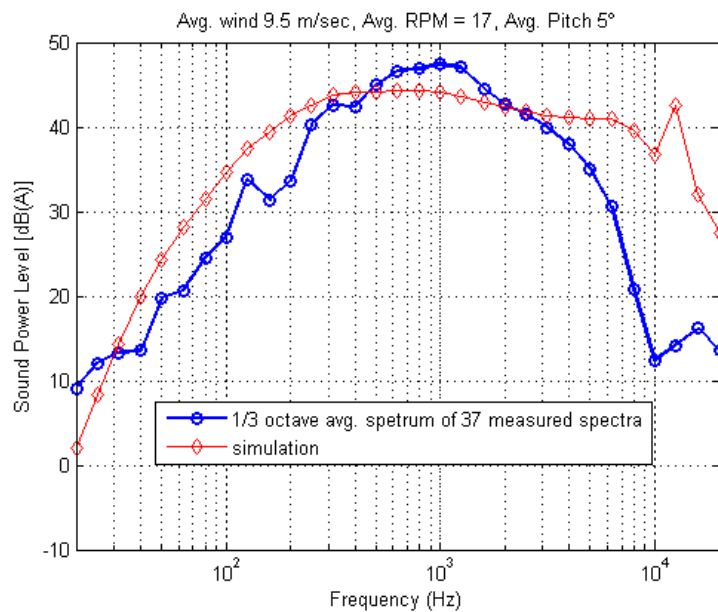


Figure 4.12: In this case the agreement for medium and low frequencies is poor in contrast to figure 4.11

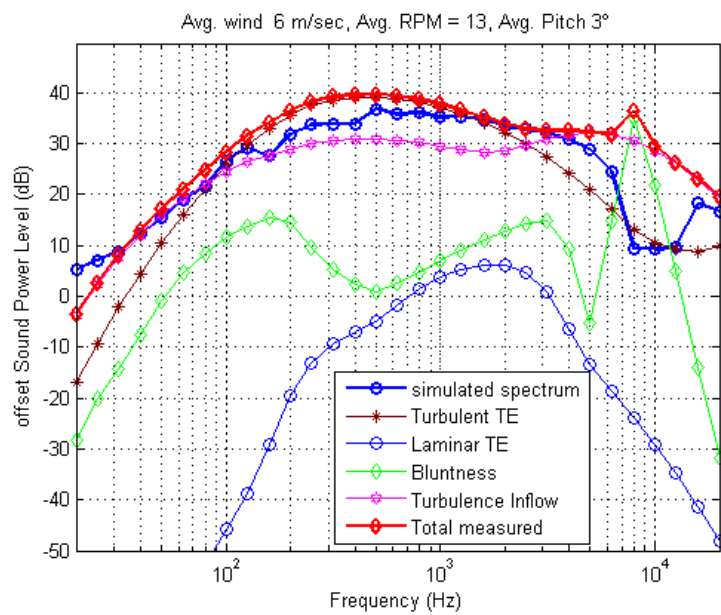


Figure 4.13: A third case, with medium-good agreement between experiment and simulation. Here the simulated noise mechanisms are also plotted individually, demonstrating the fact that the discrepancy in frequencies around 5-7 kHz is mainly due to the *bluntness* mechanism. Over 10 kHz the *turbulence inflow* noise is responsible for the overprediction

## 4.2 Rotorplane Measurements

In [11, 12] the effect of sound directivity was investigated. It was deduced that the wind turbine behaves like a *dipole* sound source. This means that there is a significant drop at the sound pressure level along the rotorplane and that the *iso*-sound pressure curves look like a reversed  $\delta$ , as can be seen in figure 4.14.

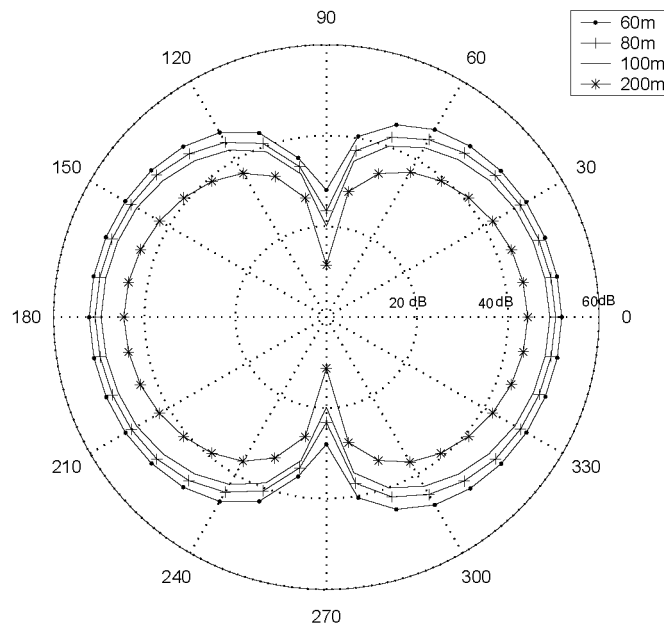


Figure 4.14: Curves of equal sound pressure at different distances and angles around a Combi 300kW turbine. It is a dipole plot. Figure adapted from [11, 12]

Since we had placed a microphone on the rotorplane, it should be easy to detect the sound pressure drop predicted by figure 4.14 and confirm the dipole properties. However, since this was not the immediate objective of our campaign at the moment, little care was taken to ensure good results. The thing is that the rotor plane does *not* remain constant with time but changes all the time since the wind turbine yaws in the changing wind direction.

This is not a problem for the downwind measurements since no big changes occur for variations of  $\pm 10^\circ$ , as can be seen in [16] and in figure 4.14. In case of the rotorplane however, good precision and synchronization is required in order to capture the drop seen in figure 4.14.

When we placed the measurement boards however, at our *estimated* rotorplane current position, a little before we started taking measurements, we did not note down the *precise* moment when this was done. In addition, the comparison that follows was made for the afternoon measurements, while the microphone was placed in the morning and was moved once during the day, when we estimated that the turbine had yawed significantly to affect the downwind measurements (again the precise time of this change was not recorded).

Therefore, it was impossible to get very accurate quantitative results, since the yaw reference angle at  $t = 0$ , could not be estimated but would always remain with an undetermined offset. Nevertheless, this offset does not prevent us from doing a qualitative investigation and still draw some interesting conclusions.

The comparison shown below is for measurements taken simultaneously at 150m downwind and at 150m on the rotorplane. The distances are equal hence direct comparison is possible. The measurements come from the Day 2,s2 time series, because this was the only time that both data files were available.

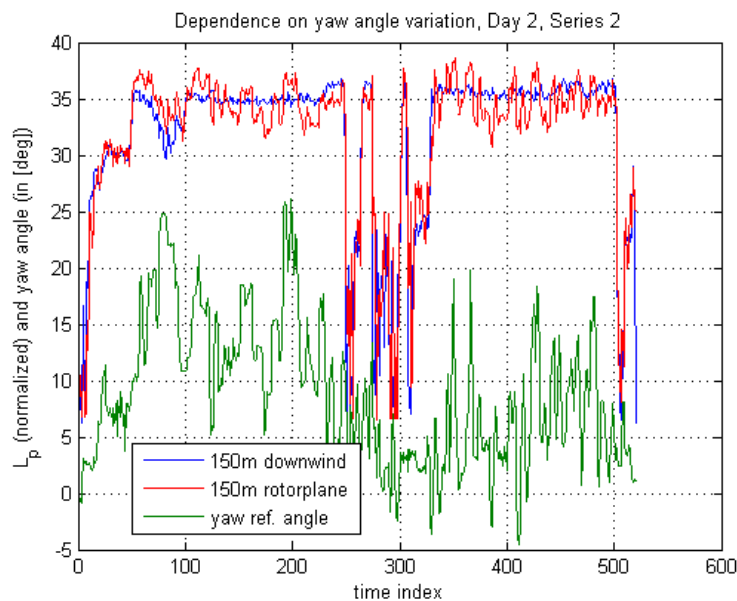


Figure 4.15: By comparing the  $L_p$  measured at two microphones placed at equal distances from the tower, we can see that the microphone placed at the rotorplane is much more sensitive in changes of the wind direction (and therefore yaw angle) than the one downwind

It should be stressed that the yaw time series has been forced to have a zero value at  $t = 0$  for visualization reasons and the *real* offset remains unknown.

What can be seen in figure 4.15 is that while the downwind time series is quite insensitive to yaw variations, the rotorplane variations follow the yaw variations very accurately. Indeed the corresponding correlation coefficients are 0.32 and 0.49 respectively, showing much higher correlation between the yaw angle and the rotorplane  $L_p$ .

Although it is difficult to say whether it is power drops we are seeing in this graph, when the microphone falls on the dipole gap, since we do not know the exact yaw angle, all the evidence point toward this fact. Anyway, it is beyond any doubt that the rotorplane measurements are very dependent on the yaw angle. A more careful study would reveal what is the exact nature of this dependence and could be target for future measurements.

A possible application of this would be to control the operation of the wind turbine in a silent mode (if the wind turbine has such a silent operation mode) with respect to the yaw angle and the observer position (possible dwellings where the wind turbine noise could be a source of annoyance). Most possibly however the yaw variations would be too quick to take advantage of such an effect.

## 4.3 Going into some details

After validating our model against our own measurements, it was interesting to test it against conclusions drawn by other peoples' research. The study in this section was partly motivated by some other experimental results published by Schepers et al. [19]. The most important of them were:

1. that the trailing edge noise is the dominant source of noise for a wind turbine,
2. that most noise is produced in the *outer part* of the blade between 75% and 95% of the span but *not* at the very tip (which might sound surprising) and
3. that most of the noise is produced when the blade is moving downwards

The measurements that led to these results, were performed on a GAMESA wind turbine, with a series of 150 microphones [19]. This gives a very good space resolution and makes it possible to locate and map the noise sources on the rotorplane. In addition, each individual blade was given a different treatment: one was left intact, one was cleaned and one was tripped. Like this, they were able to verify that the tripped blade produced more noise than the two others.

Since such a complex experimental setup was not available for this project, it was very tempting to try and validate these conclusions with our prediction model. In section 4.3.1 we present a detailed noise map along a B45 blade, while in section 4.3.2 the individual noise mechanisms were investigated. This motivated also a small parametric study of the bluntness mechanism.

As far as the third point above is concerned, the data format (10 second averages) did not permit us to investigate whether the blade produces more noise while descending. This would be possible by studying the autocorrelation function and the Fourier transform of the time series and finding the corresponding periodicities, but for such a study we needed the data in a higher sampling frequency format.

### 4.3.1 Localizing the noise

By making a separate calculation for each part of the blade, the graph in figure 4.16 was generated, showing the sound pressure contours on the rotor plane.

The plot does *not* show where on the *chord-dimension* the noise is produced. It should rather be assumed that the noise production is at the trailing edge.

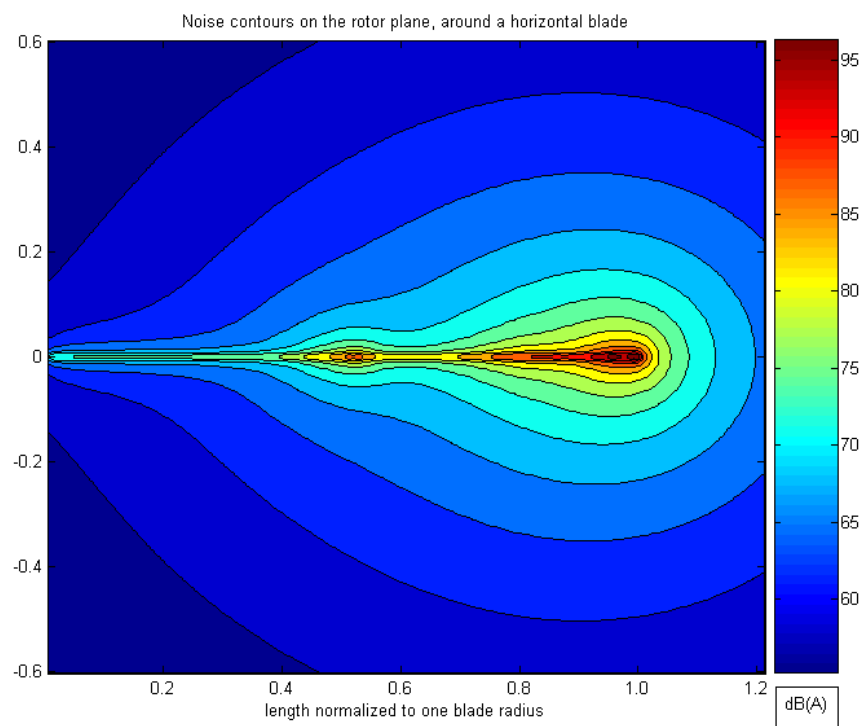


Figure 4.16: Sound Pressure level contours on the rotor plane

We make two important observations:

1. As expected, the noise is obviously produced in the outer part of the blade, where the relative velocities are higher. However, we cannot confirm Schepers et al. claim that the noise is produced from 75% to 95% of the blade. In our simulation the noise production increases up until the 3rd element from the tip, therefore almost until the 99% of the blade. Of course this can be due to differences between the GAMESA and the B45 blade.
2. Surprisingly enough, we encounter a secondary maximum of noise production in the middle of the blade! Since this is exactly the part where the blade becomes blunt (as opposed to the outer region which is rather sharp), this evidence gave rise to an investigation of the separate noise mechanisms along the B45 blade.

### 4.3.2 Identifying the noise

In figure 4.17, the spectra of the individual noise mechanisms have been plotted where calculations have only been made for the outer part of the blade (namely 75% to 99% of the span). It is not a surprise that the *Turbulent Boundary Layer Trailing Edge* noise dominates in most frequencies of the spectrum.

However, things are different for the middle part of the blade where the secondary maximum, mentioned above, occurs. In this section, there is an important contribution from the *bluntness generated* noise: it is exactly where there is a non-negligible bluntness along the span of the blade. If one trusts this result, there might be considerable improvement in the noise performance of the blade by sharpening the trailing edge of the middle part.

#### Noise mechanisms vs. wind speed

In table 4.2, we can see the evolution of several noise mechanisms with the wind speed for the SWT-2.3-92 wind turbine as computed by BEM-NOISE. Of course, this is not a strict  $Vo$ -dependency, since there is also dependency on the pitch angle and the rpm, through the corresponding pitch and rpm curves. What has been tabulated is the (broadband) sound pressure level  $L_p$  at a *non-specified* distance, so that the focus should be only at the *relative differences* between the numbers. The boundary layer separation noise is shown in different columns with the other TBL-TE mechanisms (pressure and suction side at zero angle of attack). It can be seen that it is largely responsible for the noise maximum at 11 m/sec, while it reduces considerably

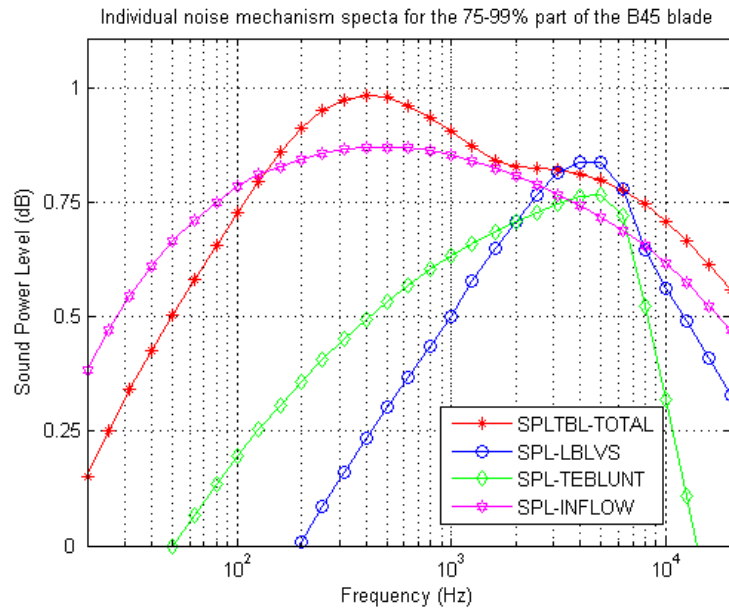


Figure 4.17: At the outer part of the blade the trailing edge noise (including the noise at non-zero angle of attack) is dominant over most frequencies

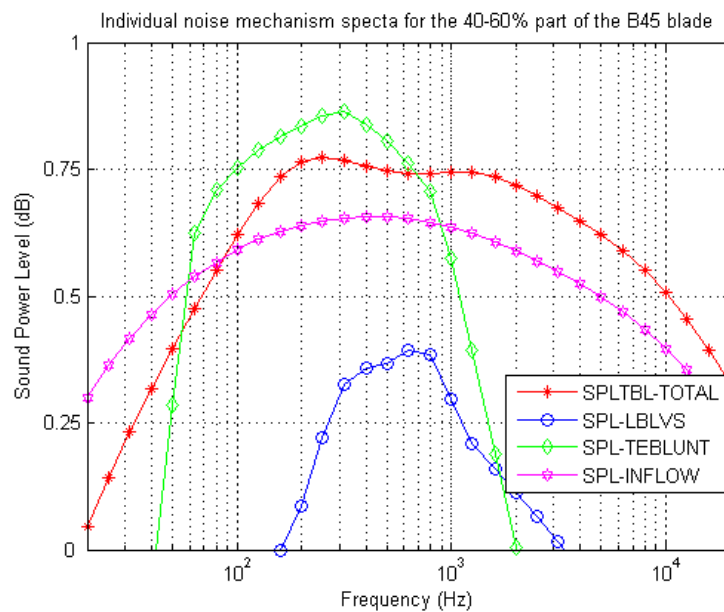


Figure 4.18: At the middle part of the blade, there is an important contribution to the noise from the trailing edge bluntness

when the machine starts pitching after this wind speed. On the other hand turbulence inflow noise remains quite constant after the rotational velocity stabilises at 9 m/sec. The bluntness mechanism can also become important. Laminar boundary layer noise and tip noise have not been included in this table, since they were found to be of minor importance.

Vo	$L_w$ tot.	separat.	turb. BL	inflow	bluntn.
5	50.0	42.8	42.1	47.6	38.9
7	59.8	55.0	53.6	55.1	49.7
9	65.5	61.8	59.1	59.1	55.9
11	66.3	64.0	58.3	59.2	54.5
13	64.4	55.3	60.0	59.3	57.0
15	64.3	47.4	60.4	59.4	58.5

Table 4.2: Study for the contribution of several mechanisms with changing wind speed.

### A study on bluntness

The above results raise some questions about the bluntness noise mechanism. The main reason is that this quantity is *not very well-defined*. Despite the fact that it is a measurable geometrical quantity, direct data for the trailing edge bluntness simply does not exist. In this study, bluntness was modeled through the 2-d airfoil profiles and their distribution along the blade together with agreement on about how it is distributed.

Furthermore, the model showed quite chaotic behavior to the bluntness variable<sup>2</sup>: by supposing that the bluntness is only 1mm more than the used one, the bluntness generated noise increases by 5 dB(A) while if it is 0.5mm less, more than 2 dB(A) less are generated (table 4.3)! At the same time the peak in the spectrum moves at lower frequencies as the bluntness increases (figure 4.19). The same chaotic behavior is observed for the trailing edge angle  $\Psi$ , which is also an input to the bluntness mechanism model. The problem with  $\Psi$  is also that it has to be deduced from the 2-d airfoil profiles.

My conclusion is that the bluntness scaling law proposed by [9] is to be treated with caution in wind turbine applications, principally for the difficulty of estimating the real value of such a sensitive variable. A new equation for this noise mechanism would be welcome, even if it was less sophisticated but more practical to apply.

---

<sup>2</sup>meaning quite big variations in the final result for small variations in the bluntness

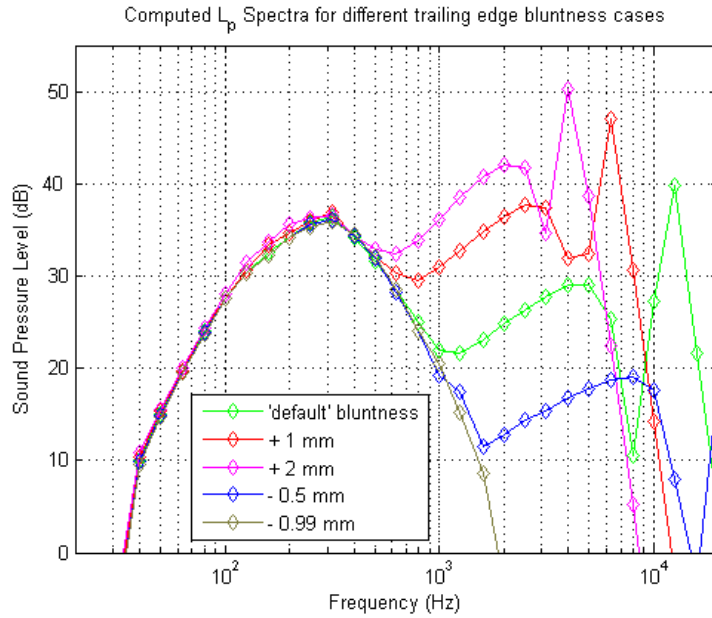


Figure 4.19: Spectra for different values of the bluntness distribution. As the outer region of the blade becomes sharper, the peak moves to higher frequencies and eventually disappears. the sound pressure level is given for a non- specified distance

	bluntness $L_p$	total $L_p$	peak location
'default'	45.3 dB	55.9 dB	12 kHz
+ 1 mm	50.0 dB	56.6 dB	6 kHz
+ 2 mm	53.0 dB	57.4 dB	4 kHz
- 0.5 mm	43.0 dB	55.7 dB	> 20 kHz
- 0.99 mm	42.8 dB	55.7 dB	-

Table 4.3: Broadband noise for the bluntness mechanism and the total noise for the bluntness parametric study. The sound pressure level  $L_p$  at an unspecified distance is presented. Notice that the bluntness contribution in the broadband noise varies a lot within 2.5 mm

# Chapter 5

## Optimization

### 5.1 Wind Turbine Settings Optimization

In figure 4.4 in section 4.1.1, we were able to see the generated noise evolves with increasing wind speed:

We observe that the noise increases fast until 9 m/sec, and then, after the rpm stabilizes at its maximum value, the rate of increase becomes slower. The noise reaches a *local maximum* at the wind speed of 11 m/sec, after which the machine starts pitching away from stall to regulate power. Then there is a clear drop in  $L_w$  due to the fact that the boundary layer separation noise becomes less important. As the wind speed continues increasing, eventually the relative velocities seen by the blade will increase and  $L_w$  will increase again. However, as it has been said before, there is no sense talking about wind turbine noise at such high wind speeds, due to the background noise. Our source of concern is clearly to reduce this local maximum at 11 m/sec and the noise at wind speeds before that.

Our purpose here is to optimize a wind turbine's performance, in this case the SWT-2.3-92, with respect to noise, by changing the combination of its operational settings ( $\omega, \vartheta_{pitch}$ ). As it can also be seen in [13], more than one optimization types can be attempted. In our report we will try two: *noise minimization* and *power maximization*. In *noise minimization*, we try to obtain a considerably lower  $L_w$  without compromising too much the power production. A strict constraint for the power would be 99% while a more relaxed would be 95% of the maximum power production. In *power maximization*, like the name implies, we try to maximize the power production, constraining however the noise not to exceed a maximum value.

We only concentrate in the interval 7-15 m/sec for two reasons: firstly, at higher wind speeds the wind turbine noise can not be easily distinguished

from the increased background noise and secondly, this interval is probably the most sensitive both in power production and in noise annoyance. We optimize the  $(\omega, \vartheta_{pitch})$  for *each* of these wind speeds separately. In order to impose a constraint at the Annual Energy Production (AEP) instead, a typical Weibull distribution is supposed, depicting the frequency of occurrence of each wind speed.

We use the optimization tool *fmincon*, provided by the MATLAB optimization toolbox. *fmincon* is used for *constrained non-linear optimization*. It tries to minimize the output value of an objective function. Here the objective function is BEM-NOISE and depending on the application, the output value can be the power or the noise production at a particular wind speed. Linear and non-linear constraints are provided to the function and these can be scalars or vectors of quantities that need to be constrained (such as maximum  $L_w$ , minimum AEP, maximum torque, etc).

An initial search point needs to be specified and, in our case, the initial search point was always the existing default operation point of SWT-2.3-92 at the given wind speed. Optionally, we can constrain the search space around it by putting bounds to it. For the individual wind speed optimizations, the runtimes were relatively low.

### 5.1.1 Noise Minimization

As explained above, in this application, we look for the combination of  $(\omega, \vartheta_{pitch})$  that lead to a less noisy operation, by constraining however the amount of power that we are willing to *trade* for this gain in noise. We performed these optimizations for two different constraints in power: 99% and 95% of the maximum power (as this is computed by the default operational settings). Optimizations were performed for all wind speeds in the interval 7-15 m/sec and the obtained gain in noise is displayed in figure 5.1. The detailed results, as well as the optimized settings that lead to these noise reductions, are given analytically in Appendix A in the form of tables and graphs.

We observe that considerable reduction in noise (2 dB) can be obtained by losing only 1% in power at wind speeds up to 9 m/sec. This gain however exhibits a minimum (0.4 dB) at 11 m/sec, which is unfortunately also the location of our maximum noise. In order to obtain significant noise reduction at this wind speed more sacrifices in power (95%) are needed.

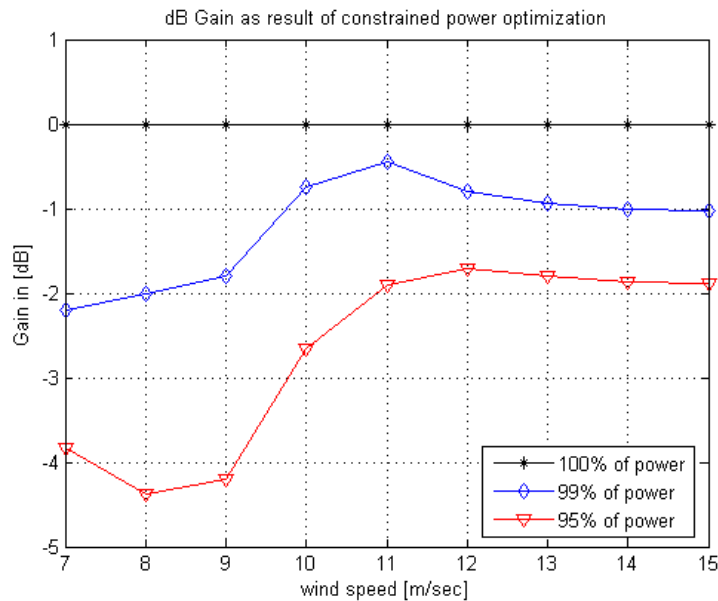


Figure 5.1: Noise reduction as a result of optimization at different wind speeds

### 5.1.2 Power Maximization

In this type of optimization, we impose an upper limit in noise and look for the optimum settings that will maximize power. This might be for example a limit that is imposed by legislation and that cannot be trespassed (in combination with the distance to the nearest dwellings). In a sense, this type of optimization is more applicable, since one might not want to lose any power at 8 m/sec, but only lose the minimum possible power at 11 m/sec. However, it presupposes that the prediction model is *super*-accurate, while the results in 5.1.1 still keep their relative value (as is also of course the case here).

We made three different attempts to constrain the maximum noise with three different noise limits and they all lead to different power curves for the SWT-2.3-92 wind turbine (figure 5.2). As it was expected, the SWT-2.3-92 will produce less and less power as the upper noise limit becomes lower and lower. We suppose here that these power curves catch up with the original power curve for wind speeds above 15 m/sec, where no constraints were imposed. We can see that it can be cheap to lower the maximum noise by only 2.2 dB, but it can become expensive to lower it some additional 4 dB.

In terms of AEP, these limits correspond to losses that can be seen in table 5.1, for a supposed site with Weibull parameters  $A = 8.5$  and  $k = 2$ .

noise constraint	-2.2 dB	-4.2 dB	-6.2 dB
rel. AEP loss	-1.34%	-6.18%	-13.71%

Table 5.1: AEP losses for different noise constraints.

In figures 5.4 and 5.5, we show *how* ( $\omega, \vartheta_{pitch}$ ) should be modified in order to achieve these *optimum* (i.e. minimum) losses. As it was expected, the main action needed is to decrease the rotational speed, combined however with some changes in the pitch angle. Figures 5.4 and 5.5 are normalized with respect to the higher default rpm and the higher and lower default pitch angle to illustrate the differences between the cases. The exact values can be found in Appendix A.

### 5.1.3 Limitations

Any optimization result value is subject to limitations, basically related to the constraints imposed to the optimization search. In our case, the optimization results were forced to obey two only extra constraints (except of course from  $L_{wmax}$  or  $P_{min}$ ). These were that the power should be regulated not to exceed 2300 kW and that the driving torque should not exceed a certain limit, which would increase the damage probability of the gear box.

Therefore no other parameters, such as load considerations, feasibility of the control system to implement the proposed changes, etc, were taken into account. Such considerations might alter these results, which are only correct in the context they have been deduced.

The method used by *fmincon* is a *sequential quadratic programming* (SQP) method. As any optimization algorithm, this might occasionally end up at a *local* minimum of the objective function [20]. However, since our search domain is rather smooth, without too many irregularities (figure 4.10), and since our results are realistic enough (we did not really expect to achieve a 10 dB reduction!), we believe that this was not the case here.

Finally, all the results presented here, depend in a way on the accuracy of the prediction model. However, even if there is an offset between prediction and reality, all the results should have a relative value. A possible exception, could be in the type of optimization where we constrain maximum noise (power maximization) and this is because some combinations of settings will not be examined at all if they lie above the noise limit. This fact will deprive them from comparison with other settings that might be less favorable, in case they should actually lie *under* the noise limit (due to an offset).

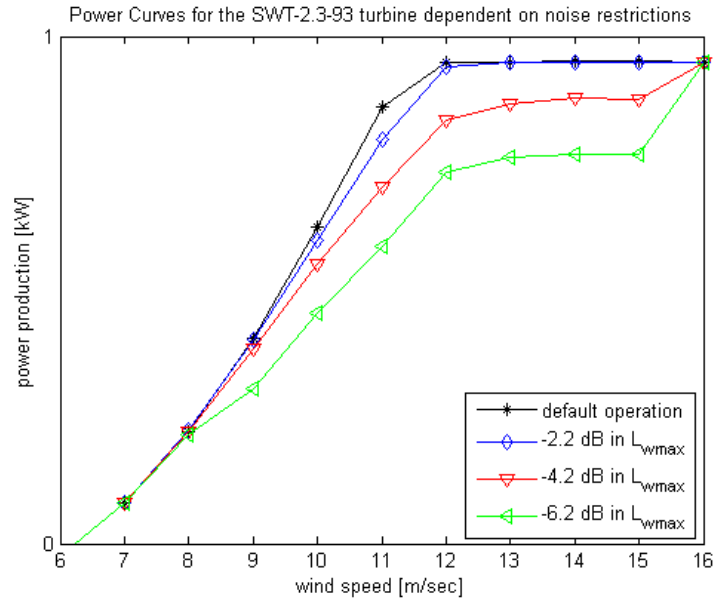


Figure 5.2: Power curves for different noise constraints

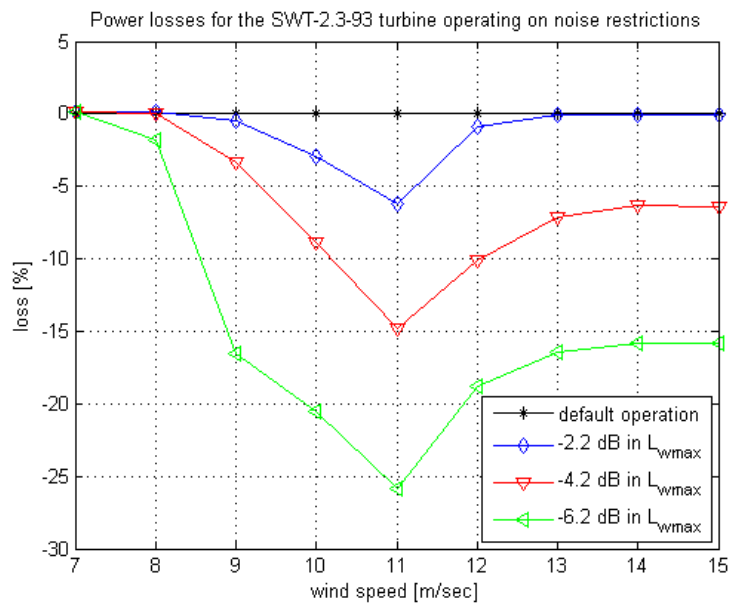


Figure 5.3: power losses (with respect to normal operation) for different maximum noise constraints

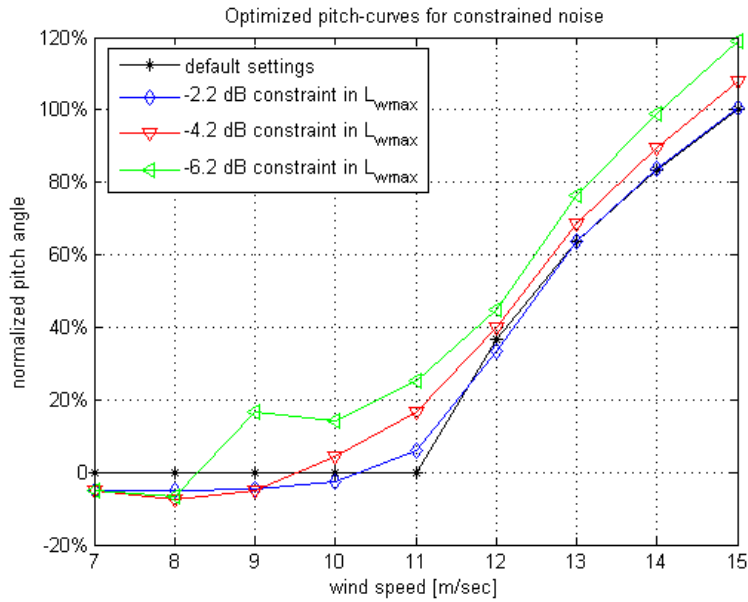


Figure 5.4: Pitch settings (normalized) that give optimum solutions for noise restrictions

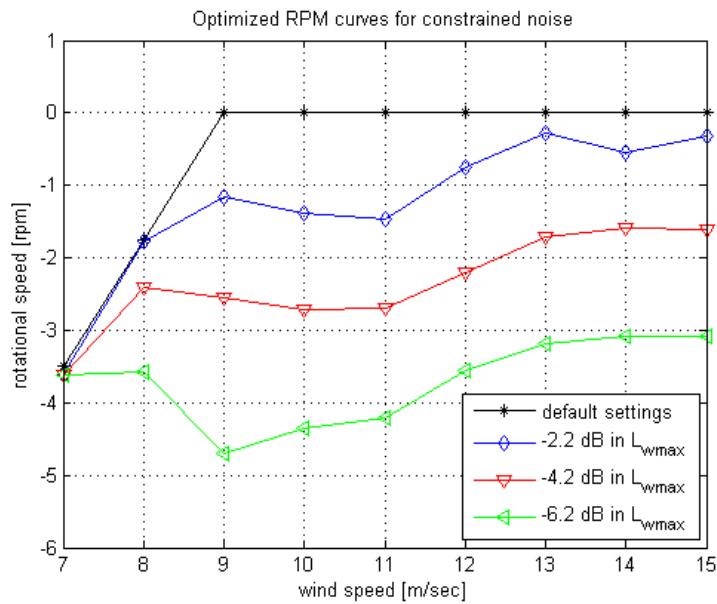


Figure 5.5: Rpm settings (normalized) that give optimum solutions for noise restrictions

## 5.2 Wind Turbine Blade Optimization

In section 5.1, we optimized the *existing* wind turbine to operate more silently by changing parameters that are easy to control such as the rotational velocity and the pitch angle. It was therefore an optimization with results that could be applied *immediately*. In this section, it is our purpose to go a little further: that is to optimize the wind turbine rotor itself. Similar optimizations with respect to noise have been made before in [13].

In this study we are going to examine the following variables: the chord, the twist and the relative thickness distributions.

By modifying slightly the existing distributions of the B45 blade, we want to see if we can obtain a more silent rotor. In order to examine the individual influence of *each* one of the variables, we will first modify each distribution separately (i.e. optimize the twist by keeping chord and relative thickness constant and so on). In the end, one big optimization with all the parameters will be attempted.

As in section 5.1, we perform two types of optimization: noise minimization and power maximization. Again all optimizations were made by use of the *fmincon* optimization tool coupled with BEM-NOISE.

It should be stressed that this was a pure *noise and power* optimization. It therefore involves no other parameters that influence blade design, such as load considerations, cost limitations or manufacturing feasibility. Especially loads are particularly important for the calculation of the blade lifetime, fatigue and, hence, can directly influence the cost of the wind turbine. Our results have therefore their limitations, and they could be improved in a future study.

Nevertheless, our conclusions can still provide important guidelines in the wind turbine design procedure when noise considerations need to be taken into account. It can be directly checked whether the proposed distributions influence negatively the performance of the blade in another field.

Unlike section 5.1, in the blade geometry optimization there is no sense optimizing at each wind speed separately. Therefore, our optimization target (or constraint) should be the AEP for a given Weibull distribution.

Due to both the increased number of wind speeds and the increased number of variables, the runtimes increase considerably compared to section 5.1. For this reason, we had to find ways to reduce them.

As a first step, the optimizations were performed for wind speeds up to 11 m/sec. It was supposed that beyond that wind speed, there would always exist a pitch angle that would regulate power to 2300 kW, so this would not affect the AEP calculations. In addition, the maximum noise (which we want to minimize) is also located at 11 m/sec and wind speeds after this will not

affect the noise minimization calculations.

As a second step the variable distributions had to be reduced to a handful of elements. BEM-NOISE divides the 46.2m B45 blade into 100-150 elements to achieve convergence in the noise calculations. If so many variables were input to *fmincon*, for every (!) trial, the runtimes would certainly become (beyond) unacceptable. For these reasons, the twist, chord and relative thickness distributions were *reduced* to a grid of few points along the span, which were connected with a *spline*. Then BEM-NOISE performed its calculations in 100 elements interpolated along this spline. Of course, we applied a grid that is finer toward the tip, since both power and noise generation are most sensitive near the tip.

Finally, it became apparent after the first tries, that it was very difficult to control the behavior of the root of the blade without explicit constraints that were outside our domain of interest for this project (loads, manufacturing ability, etc). Anyway, it is the geometry of the *outer part* that influences mostly power and noise generation. For this reason, we decided to restrict our optimization efforts to this part. This, of course, would allow us to be more economic in our computations, as well. Thus, our first computational node, was set approximately at 1/3 of the blade radius.

In section 5.2.1 the twist distribution is optimized, while in sections 5.2.2 and 5.2.3 we optimize chord and relative distributions respectively. Section 5.2.4 includes our big optimization and in 5.2.5 we sum up our conclusions.

### 5.2.1 Twist optimization

For the twist optimizations we applied the following constraints:

1. the twist was forced to zero at a point near the tip, in order to keep some resemblance with the B45 blade
2. the twist had to decrease monotonically until this zero point
3. the twist was not allowed to exceed  $20^\circ$  or become less than  $-10^\circ$
4. the produced power should not exceed 2300 kW
5. the driving torque should not exceed the limit mentioned in 5.1.3
6. the AEP was not allowed to fall beyond 99% of the already existing (for noise minimization) while the  $L_{wmax}$  was not allowed to increase more than the existing value (for power maximization)

Of course, some of these constraints (such as the torque) remained inactive during the twist optimization, but they are stated for completeness.

The results of both types of optimizations can be seen in figure 5.6 and table 5.2

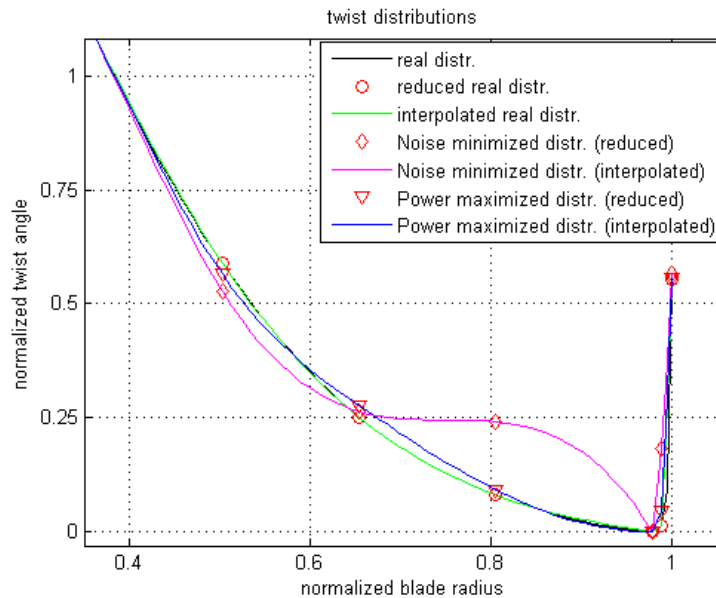


Figure 5.6: Original and optimized twist distributions zoomed in the outer part of the blade (further in the distributions are identical). The magenta line is the distribution obtained by noise minimization while the blue line is the result of power optimization. It is not very different than the *real* existing distribution (black line). In order to make the calculations, the distributions were reduced to 6 points connected with splines. As can be seen, in the case of the real distribution, this is a reasonably accurate approximation since the green line (spline simulating the real distribution) and the black line (real distribution) are almost identical

It seems that with the current constraints we cannot obtain a significant noise reduction by changing the twist distribution alone: just 0.45 dB(A). At least one can say that this reduction was achieved at almost no cost: only 0.6% of the AEP was the penalty for this reduction.

Since it was obvious, from the *noise minimization*, that not much noise could be gained, there was no point imposing a very strict noise constraint for the *power optimization*. So we just did not allow it to increase more. It became apparent that the twist converged relatively fast very near its previous value (black curve in figure 5.6). In a sense, this should not surprise

method	Gain in AEP	Gain in $L_w$
<i>noise min.</i>	-0.60%	-0.45 dB
<i>power max.</i>	+ 0.04%	-0.0 dB

Table 5.2: Twist optimization results for two different methods

us because the twist of the SWT-2.3-92 machine *is* power optimized. So this also validates in a way our optimization method.

### 5.2.2 Chord optimization

Compared to the twist angle, optimizing the chord involves a few more complications. The first one is that the longest the chord, the bigger the lift and therefore the more the produced power. Thus, if left unconstrained, the chord tends to increase indefinitely to boost the power production. This leads in blades that are definitely non-feasible. As a matter of fact, for as many explicit and implicit constraints we attempted, this was the case. Soon the constraints had to become so strict that the blade was rather *forced* than optimized. Therefore, we decided to perform only *noise minimization* when varying the chord distribution.

In addition, the chord  $c$  is directly linked to the relative thickness  $t$  through the *absolute* thickness  $a$ :

$$a = t \cdot c \quad (5.1)$$

So if the relative thickness is kept constant, the absolute thickness is modified proportionally to the chord. This induces an additional constraint to our optimizations because we want our absolute thickness to decrease monotonically (such a demand is not mandatory for the *relative* thickness).

Another thing that changes following the chord distribution is also the trailing edge *bluntness* distribution and all these changes need to be taken into account.

To sum up, the constraints used, in addition to those in 5.2.1, were:

1. the absolute thickness had to decrease monotonically
2. the chord had also to decrease after its maximum value. Since this value was located before the part of the blade we were interested in, the chord had to decrease everywhere in our domain
3. a constraint was imposed to the blade mass so that it would not increase beyond a certain limit

4. finally, another constraint was imposed to the AEP, to prevent the chord from increasing more: we actually did not allow the AEP to increase more than 1%! This might sound weird in power maximization and this is why constraints in *loads* have to be applied instead.

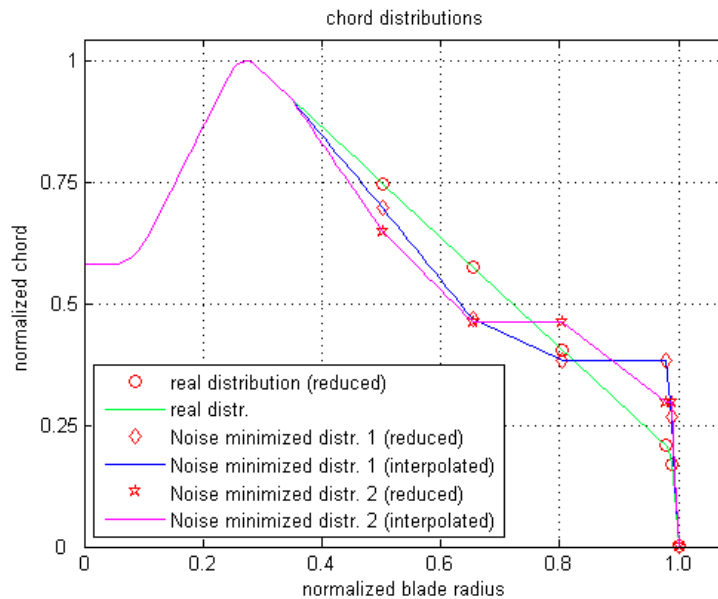


Figure 5.7: The original chord distribution (normalized) and two different chord optimizations from noise minimization, obtained by different constraints near the tip region.

In figure 5.7, we have plotted two different chord distributions that minimize noise. Their difference is that a stricter constraint was imposed to the magenta curve near the tip. Both distributions give a more significant noise reduction than the change in the twist distribution, namely 0.75 dB. This is again not a number that by itself is impressive but what is more interesting is that it is actually combined with an *increase* in power. So we get two in one! This is a reason to further investigate this modification in the future.

method	Gain in AEP	Gain in $L_w$
<i>noise min.</i>	+1.00%	-0.76 dB

Table 5.3: Chord optimization results for noise minimization optimization

### 5.2.3 Relative thickness optimization

It has not been said directly, but it is evident that within this optimization we did not want to change the airfoil types used in the B45 blade. This would be a very complicated task.

However, changing the relative thickness, will change the distribution of these *given* airfoil profiles along the blade. For example, a hypothetical *22% thickness airfoil* that was used at a span  $x$  in the B45 blade, where the relative thickness was obviously 22%, would change position and would be situated now at a *different* span  $y$  in the optimized blade (at the position where the relative thickness would be 22% again). This induces some complications and proper care has to be taken both for the power and the noise computations. The reason is that all the interpolations between the different stations of the blade concerning *both* the boundary layer thickness distributions *and* the lift and drag coefficient curves, have to be modified accordingly.

Having stressed this, no further constraints need to be applied to our optimizations, except from the demand that the relative thickness at the tip has to remain unchanged.

It turned out that the results we obtained both for noise minimization and power maximization, were not that exciting: no big changes could be obtained by variation of the relative thickness (at least with the existing constraints)

### 5.2.4 All variables optimization

Having performed an all-variables-separately optimization, it was interesting to see whether we could combine the reduction gained by twist and chord separately, to obtain a significant reduction, combined possibly with an increase in power production. This would be the ideal outcome for such a project. It was also interesting to see whether the individual variables would follow the same trends as when optimized separately.

#### Noise Minimization

The results for noise minimization can be seen in figures 5.8, 5.9 and 5.10. We performed two optimizations. One for dividing the outer part of the blade in 4 parts (first attempt) and one in 6 parts (like in the individual optimizations). The reason why we did not attempt the 6 point division directly, is that this time the computational time is increased by a factor of 3 (because we get 6+6+6 variables for each distribution). For this reason, we tried first a lighter version with 4+4+4 variables. The reason that they are both displayed here

is to demonstrate their similarities. Despite the fact that more accuracy is attained with 6 points, the distribution had the same tendencies: a slight increase in the twist angle, and a relative reduction of the chord in the middle part, combined with a slightly thicker chord near the tip. Of course the 4-point picture is more *rough*, but it is a good sign for our optimization technique that the two distributions seem to converge. Better accuracy would be obtained with a finer grid and this is only a question of computational time (not of any method limitations). This could be attempted in a future project where more computational time is available.

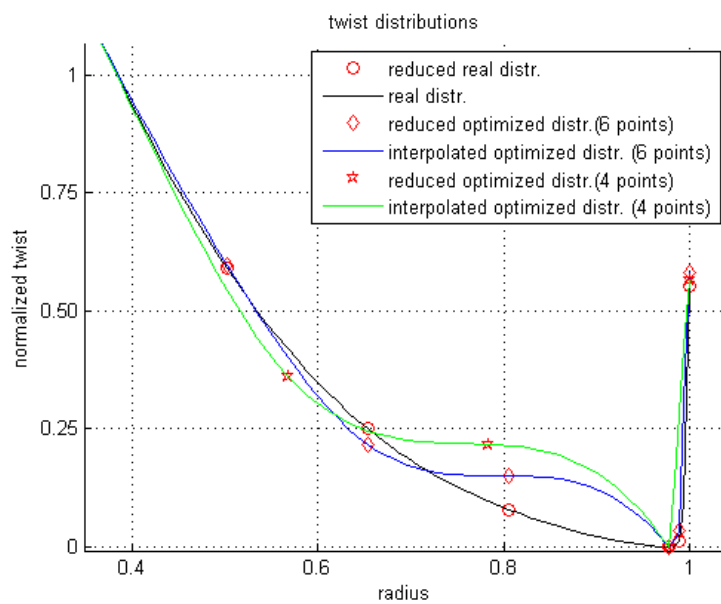


Figure 5.8: Results of blade optimization in twist

In total, a 1 dB reduction was obtained together with an *increase* in power by 1% by changing the blade *only*. This is a significant result especially if it is combined with the results in 5.1, where  $\omega$  is allowed to vary to obtain further noise reductions. With the increased power produced by the blade, we can loosen the constraints and have a much quieter blade producing at the same rate.

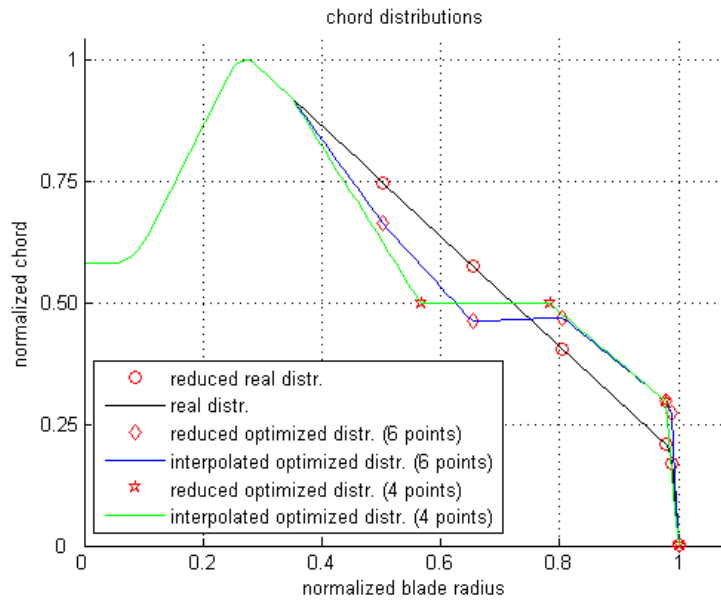


Figure 5.9: Results of blade optimization in chord

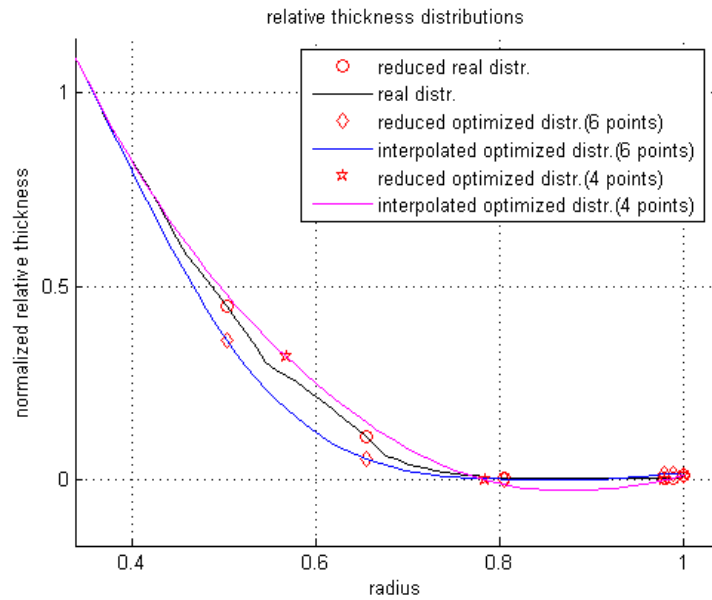


Figure 5.10: Results of blade optimization in rel. thickness

method	Gain in AEP	Gain in $L_w$	Blade mass
<i>noise min.</i> (6 points)	+1.00%	-1.0 dB	-3.92%
<i>noise min.</i> (4 points)	+ 0.96%	-1.0 dB	-4.00%
<i>power max.</i> (4 points)	+ 5.19%	-1.0 dB	+2.93%

Table 5.4: Results of the blade optimization with two different methods and two different grids

### Power Maximization

The corresponding results for power maximization can be seen in figures 5.11 and 5.12 (the relative thickness does not change significantly). As explained in the chord section, these results are marked by the tendency of the chord (and hence mass and loads) to increase. So the results have to be treated with caution. We believe that for this kind of optimization proper explicit constraints by load considerations have to be applied in order to get meaningful results. Since it was clear where these computations were leading to, no extra time was attempted in refining the grid.

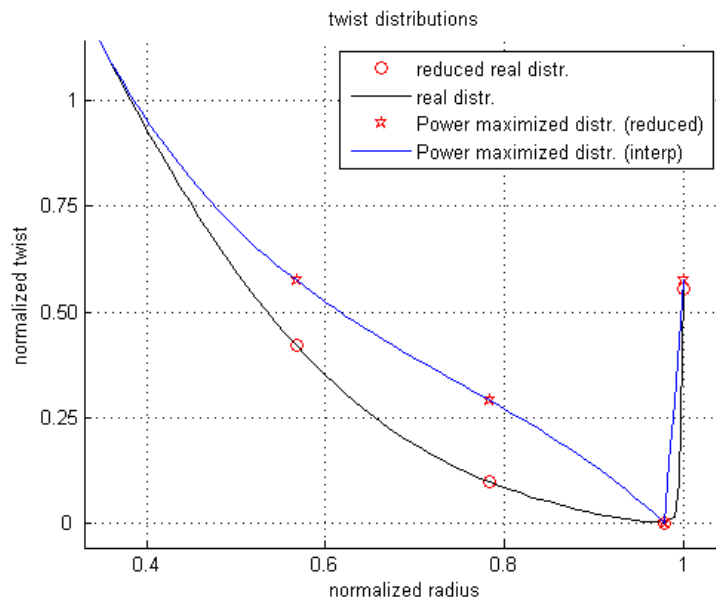


Figure 5.11: Twist distribution for power maximized blade

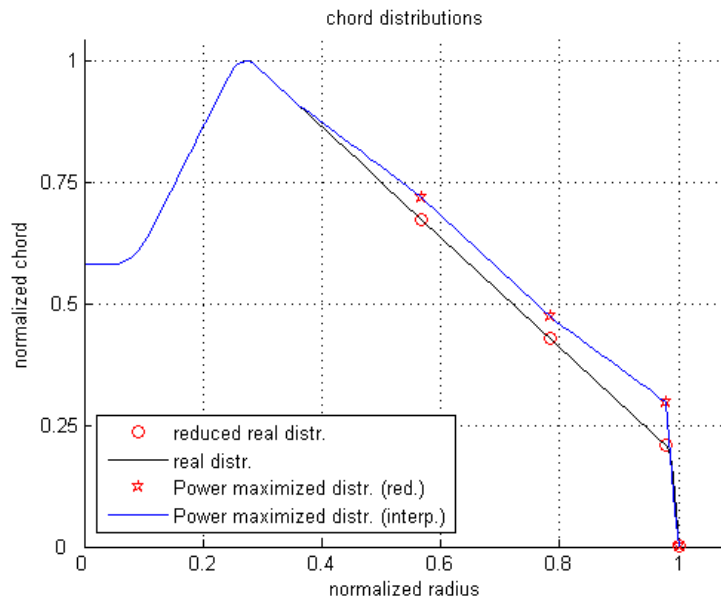


Figure 5.12: Chord distribution for power maximized blade

### 5.2.5 Summary

By optimizing the B45 blade we were able to achieve both a noise reduction by 1 dB and an increase in the AEP by 1%. We believe that these results are significant. These results were obtained by the *noise minimization* optimization type. The *power maximization* gives some theoretically better results (+ 5% in power) which are however combined with an increase in the chord and therefore in the blade mass.

# Chapter 6

## Conclusions

This project dealt with predicting and minimizing wind turbine noise. Both simulations and measurements were used in this direction. A code predicting noise and power output simultaneously was developed, based largely on an already existing noise generation model.

Detailed noise data, at different rotational velocities and different pitch angles, was collected at the SIEMENS SWT-2.3-92 wind turbine at Høvsøre. This data was used to scrutinize the model's performance and the model proved to be doing fairly well: it seemed to predict accurately the wind turbine's noise behavior at its default operation mode, against rpm variations and against pitch angle variations at high rpm. Against pitch angle variations at low and medium rpm, our model overshoots measurements considerably. However, there is evidence that it is the particular set of measurements that is responsible for this. As far as spectra are concerned, our model predicts more or less well the spectrum shape up to frequencies of 3 kHz. Above that there are deviations.

The individual noise mechanisms were studied separately, revealing the high contribution of the separation-stall mechanism at the noise maximum, and a detailed noise map along the blade was computed, motivating also a study on the bluntness mechanism.

An important correlation between the sound pressure at the rotorplane and the yaw angle variations was observed, probably confirming previous suggestions that the wind turbine behaves like a dipole source.

As a next step, the code was coupled to an optimization tool and was first used for optimizing the wind turbine's operational settings. This was done for a series of wind speeds and for two different optimization targets. For some wind speeds considerable reductions in noise can be obtained at low cost. As we approach the noise maximum however, or if the noise constraints become tight, more power is lost. This kind of optimization can lead to a more quiet

operation of *existing* variable speed, pitch regulated wind turbines. It can also be of use in particular situations, where noise limits have to be met or when a wind turbine needs to operate in a secondary silent mode.

Finally, the wind turbine blade itself was optimized: a more silent rotor was produced by modifying mainly the chord and twist distributions. This noise reduction was combined with an increase in the AEP. Although these conclusions have some limitations, they could be used in the future as guidelines to more silent blade designs when load considerations are taken into account as well.

# Appendix A

## Optimized Settings

Appendix A is available with permission of SIEMENS WIND POWER A/S

# Bibliography

- [1] Danish Wind Energy Association, *Sound from Wind Turbines*, <http://www.windpower.org/en/tour/env/sound.htm>
- [2] British Wind Energy Association, *Noise from Wind Turbines - The Facts*, <http://www.britishwindenergy.co.uk/ref/noise.html>
- [3] Van den Berg, G. P., 2004, *Effects of the wind profile at night on wind turbine sound*, *Journal of Sound and Vibration*, **277**, 4-5, pp. 955-970
- [4] *First and Second International Conference on Wind Turbine Noise* <http://www.windturbinenoise2005.org/>
- [5] Grosveld, F. W., 1985, *Prediction of Broadband noise from Horizontal Axis Wind Turbines*, *Journal of Propulsion and Power*, 1, pp. 292-299
- [6] de Wolf, W. B., 1986, Een predictiemethod voor her aerodynamische geluid van winddurbines met horizontale AS. NLR TR 87018 L, pp. 1-55
- [7] Viterna, L. A. The NASA LeRC Wind Turbine Prediction Code. NASA CP-2185, pp. 410-418
- [8] Shen, W. Z., Sørensen, J. N., 2001, *Aeroacoustic Modeling of Turbulent Airfoil Flows*, *AIAA Journal*, **39**, 6
- [9] Brooks, T. F., Pope, D. S. and Marcolini M. A., 1989, *Airfoil Self-Noise and Prediction*, NASA Reference Publication 1218, National Aeronautics and Space Administration, USA.
- [10] Amiet, R. K., 1975, *Acoustic Radiation From an Airfoil in a Turbulent Stream*, *J. Sound Vib.*, **41**, pp 407-420.
- [11] Zhu, W. J., 2003, *Modeling of Noise from Wind Turbines*, Master Thesis, Technical University of Denmark

- 
- [12] Zhu, W. J., Heilskov, N., Shen, W. Z., Sørensen, J. N., 2005, *Modeling of Aerodynamically Generated Noise from Wind Turbines*, Journal of Solar Energy Engineering, **127**, pp 517-528
- [13] Fuglsang, P., Madsen, H. A., 1996, *Implementation and Verification of an Aeroacoustic Noise Prediction Model for Wind Turbines*, Risø National Laboratory publication R-867(EN)
- [14] Moriarty, P., Migliore, P., 2003, *Semi-Empirical Aeroacoustic Noise Prediction Code for Wind Turbines*, National Renewable Energy Laboratory publication NREL/TP-500-34478
- [15] Drela, M. 1989, *XFOIL: An analysis and Design System for Low Reynolds Number Airfoils*. Conference on Low Reynolds Number Aerodynamics. University Notre Dame.
- [16] International Electrotechnical Commission, *IEC 61400-11 Standard: Wind Turbine Generator Systems - Part 11: Acoustic Noise Measurement Techniques*, Document No. 88/166/FDIS
- [17] Brüel and Kjær, *Measuring Wind Turbine Noise with PULSE*, <http://www.bksv.com/2939.asp>
- [18] Jakobsen, J., Andersen, B., 1993, *Aerodynamical Noise from Wind turbine Generators*, Danish Acoustical Institut, 1993-06-04, LI 464/93 D/70.89-464.1
- [19] Schepers J. G., Curvers, A. P. W. M., Oerlemans, S., Braun, K., Lutz, T., Herrig, A., Wuerz, W., Méndez López, B., 2005, *SIROCCO: Silent ROTors by aCOustic Optimalisation*, First International Meeting on Wind Turbine Noise: Perspectives for Control
- [20] The MATLAB Help Manual, *Optimization Toolbox, fmincon*, The Mathworks, Inc.